CENTRO DE INVESTIGACIONES
EN OPTICA, A.C.

“OPTOMECHATRONIC DEVICE TO CLASSIFY MONOCHROME DERMATOLOGICAL IMAGES SUPPORTED BY RGB-STOKES POLARIMETRIC ANALYSIS”

A thesis submitted in partial fulfillment of the requirements for the degree of Master of Optomechatronics.

Presented by: Oscar Ismael Rodríguez Cortés, B. Eng.

Advisor: Geminiano Donaciano Martínez Ponce, Ph. D.

León · Guanajuato · México
October 2024

Acknowledgments

First and foremost, I would like to thank God for granting me all the opportunities that have led me to this moment.

I am deeply grateful to my mother for her unwavering support, and to my sister for her constant motivation.

I extend my heartfelt thanks to PhD Geminiano for his invaluable guidance and mentorship, and to my lab colleagues for their advice.

I also want to express my appreciation to my friends, especially Luis, Dixie and Ingrid, and everyone who has supported me, whether directly or indirectly.

I am sincerely grateful to CONAHCYT for their financial support that made this work possible, and to CIO for providing all the necessary tools.

Dedicated To,

My mother, Dr. Hortencia Cortés

Abstract

Melanoma, the deadliest skin cancer, demands enhanced diagnosis methods to decrease uncertainty in disease identification. In this regard, an imaging optomechatronic device herein is developed that integrates an automated standard clinical prediction rule (CPR) and polarimetric images with the aim of building a novel database and to assist physicians in diagnosing skin conditions with a broader information base. Through multispectral Stokes imaging polarimetry using a polarized light source (circular/linear polarizations), an image set of polarization features, such as Degree of Linear Polarization (DoLP) and Degree of Circular Polarization (DoCP), are calculated. The implemented CPR is the ABCDE rule, which classifies skin lesions based on Asymmetry, Border, Color, Diameter, and Evolving. The device uses an addressable RGB LED ring lamp with the appropriate polarization filter to highlight skin lesion features. Diffusely reflected light is collected, passed through a Stokes polarimetric setup, and digitized by a monochromatic CMOS sensor. The system captures images for the ABCDE process and performs the polarimetric process, synchronizing the rotation of the quarter-wave plate with frame acquisition. The resulting images show the degree of polarization for different spectral ranges. By integrating polarimetric imaging and machine learning, this handheld device aims to improve the quality of melanoma diagnosis, offering a user-friendly and portable tool for physicians.

Contents

List of Figures

Chapter 1

Introduction

The skin, the largest human organ, covers the entire body surface. Skin characteristics, such as thickness among many others, depend on the analyzed body region, age, gender, ethnicity and even lifestyle. [1] Skin is mostly divided in three layers: epidermis, dermis and hypodermis. The first one is divided in five sublayers or strata: stratum corneum, stratum lucidum, stratum granulosum, stratum spinosum and stratum basale. The second skin layer comprises the papillary layer and the reticular layer. Finally, the one at the bottom, the hypodermis consists in loose connective tissue (subcutaneous fat) and blood vessels. [2] This intricated structure protect the body against pathogens, ultraviolet (UV) light, chemicals, and mechanical injury. This organ also regulates temperature and the amount of water released into the environment. [3]

Owing to depletion of the stratospheric ozone layer, the Global Horizontal Irradiance (GHI) is slightly increasing due to a larger UV-irradiation component. In particular, prolonged skin exposure to the UV-B waveband (280-320 nm) is responsible for the induction of nongenetic malignant melanoma mainly in white skin human beings. On the other hand, even though sunscreen use is rising, the incidence of melanoma continues to increase, suggesting that current preventive measures may be insufficient or not effectively implemented. This highlights the need for better protection strategies, a better understanding of the risks of UV exposure, and the development of new technologies for the prevention and diagnosis of skin cancer. [4] This is the problem that forms the basis of this thesis project: **the design and development of a medical device that helps improve, in a non-invasive way, the**

diagnosis of melanoma.

The project involves the development of a device for acquiring RGB and polarimetric images of skin lesions (moles) that will be digitally processed. The generated information aims to reduce uncertainty in the diagnosis made by the specialist doctor. The value proposition consists of combining the analysis of nevi using the ABCDE rule by applying digital processing of RGB images and the analysis of polarimetric Stokes images in different spectral intervals to identify characteristics associated with skin structure and its stages in various pathologies.

1.1 Melanoma

Melanoma, which means "black tumor", is a malignancy derived from skin cells called melanocytes, which are contained in the stratum basale. These cells are responsible for producing melanin, the pigment that gives skin its color. If not detected early, melanoma can easily spread to other parts of the body, causing metastasis, making it one of the most dangerous forms of skin cancer. Early diagnosis and treatment are crucial for improving patient outcomes.

Malignant melanoma, although far less prevalent than non-melanoma skin cancers, is the main cause of skin cancer death and is more likely to be reported and accurately diagnosed than non-melanoma skin cancers. According to the World Health Organization, between 2 and 3 million non-melanoma skin cancers and 132,000 melanoma skin cancers occur worldwide each year [5]. The best way to prevent death from any type of cancer is to have a correct and early diagnosis, so that treatment begins in the early stages of the affection. Elderly male persons, mainly of European ancestry, are the group with the highest incidence of melanoma. [6]

This thesis proposes the design, development and evaluation of an optomechatronic device, capable of using polarimetric imaging and automated image processing to facilitate the diagnosis of melanoma and to give the dermatologist more information of the skin, whithout relying only on the visual perception of the nevus state and the experience of the physician.

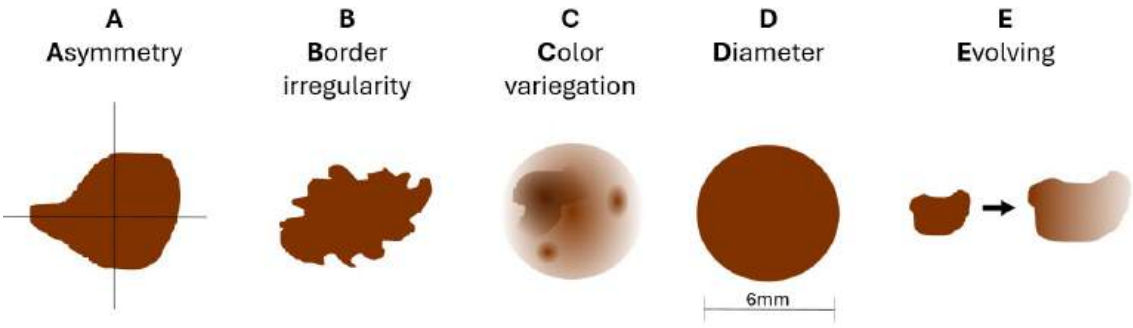

Figure 1.1 – ABCDE Rule for melanoma detection.

1.1.1 ABCDE Rule

The ABCDE criteria, shown in figure (1.1) was devised and popularized in the mid-1980s to create a simple yet effective method for people and physicians to analyze melanoma's clinical features [7]. This tool is a simple, easy-to-remember mnemonic that includes Asymmetry (A), Border irregularity (B), Color variegation (C), Diameter larger than 6mm (D), and Evolution over time (E). Interestingly, the ABCDE criteria was not derived from statistical evidence, but rather from the best judgements of expert clinicians. Thus, making it empirical knowledge. [8] ABCDE rule scoring is not sufficient to diagnose malignant melanoma and it should be complemented with detailed clinical history and regular full body examination assisted by dermoscopy. Besides, this rule should be taught to patients with the aim of increasing attention and identification of abnormal skin lesions. [9] Another clinical prediction rule that overlap features with ABCDE for assessing pigmented skin lesions with the naked eye is the seven point checklist (7PCL). Change in size, irregular shape or border and irregular color are considered major features. On the other hand, largest diameter 7 mm or more, inflammation, oozing or crusting of the lesion and change in sensation (including itch) are pondered as minor features. [10]

There are other measures that specialized physicians employ to evaluate melanoma invasion degree: The Breslow depth and the Clark level. The former measures melanoma sample from the skin surface down through to the deepest tumour point with a micrometer and microscope, thus, it is an invasive test. The latter had five levels which are defined considering the layers invaded by melanoma. Both measures are still included into the more general American Joint Committee on Cancer (AJCC) staging system. Nonetheless,

the definition of this progonostic staging protocol is beyond the scope of this study. [11]

1.2 Dermatoscopy

Currently, the most common way physicians analyze moles is through the ABCDE rule; however, nowadays there is enough technology to transition toward a more advanced and precise analysis. A non-invasive, enhanced analysis of moles can be achieved by using specialized cameras, imaging techniques, and even computational methods such as Deep Learning. This approach quantifies ABCDE parameters and unveils traits and characteristics that are not discernible to the naked eye.

Several studies have suggested that dermatological screenings can correlate with earlier detection of melanomas and improved prognosis. Various pilot programs deployed in Europe to measure the effects of large-scale skin cancer screening initiatives at the primary care level have shown the potential to reduce patient treatment costs and mortality when performing full-body examinations in large numbers of high-risk individuals. [12] Recent efforts to develop open repositories to train artificial intelligence (AI) algorithms to classify skin lesions are found in the world wide web. [13, 14, 15] Regrettably, there is a lot of work ahead in order to homogenize relevant features in filed images: resolution, bit depth, illumination, etc.

1.3 Purpose of the study

The technological process described herein consists in designing, constructing and evaluating an improved version of a preliminary polarimetric imaging model achieved by our research group [16]. In this regard, innovative features have been devised after a competitive analysis that help us as a guideline to add advantages and differentiating factors in the current dermatoscope prototype [17].

The specific objectives of this study are:

- Evaluate different types of illumination (laser or LED) and types of polarized light for the characterization of biological tissue using the Stokes polarimetry technique.

- Implement image processing algorithms to identify characteristic features of dermatological lesions based on the ABCDE rule.
- Design an optical imaging system free from vignetting and other optical aberrations to maximize the instrument's field of view.
- Identify and implement components to enhance the device application capabilities.
- Develop a prototype that achieves a technological maturity level 5.

In general, the main purpose is contributing to develop national technology that supports activities of healthcare professionals based on value propositions. Likewise, promote national technological independence through the generation of intangible capital (knowledge).

Chapter 2

Review of the literature

2.1 Existing technology

For the diagnosis of melanoma, there have been several advances in dermatoscopic technology in recent years, focusing mainly on noninvasive devices that provide physicians with more detailed information about the skin. Most of the commercially available dermatoscopes include only two basic functions: illuminating the skin and augmenting the image. Light sources are predominantly white LED-based lamps arranged in a circle. On the other hand, amplification can be achieved either with an amplifying lens and the eye or by projecting the image captured with a digital camera on a screen.

In the dermatological device market, those that use polarized light offer significant advantages. These devices reduce skin glare (the reflection of the skin surface), providing more in-depth images. In addition, the structures of melanocytes become more visible due to the depolarization caused by melanocytes (cells responsible for the color of the skin). An example of a commercially available dermatoscope featuring this technology is the DermLite DL200 Hybrid (Figure 2.1), which has a price of $10,050 USD. This device also includes white ilumination and image amplification.

There are also research publications that present devices which include Stokes polarimetric technology to study the skin. One example is shown in Figure 2.2, which can obtain Stokes parameters and the Degree of Polarization (DoP) of the skin surface.

A multispectral polarimetric dermatoscope using two rotating elements to analyzed dif-

Figure 2.1 – Commercial dermatoscope DermLite DL200 Hybrid, features polarized illumination

Figure 2.2 – Stokes dermatoscope developed by Daniel C. et al. (2018)

Figure 2.3 – Multispectral polarimetric dermatoscope using two rotating polarizing elements.

fuse reflected light from the skin was developed previously (Figure 2.3). The developed prototype delivered the four imaging Stokes parameters when blue, green and red Dual In-line Package (DIP) LEDs were used as illumination sources. In order to avoid resistor image on the skin, an optical diffuser was used as well as a linear polarizing film. Control software was developed under the Labview programming environment. [16]

2.2 Recent research publications about similar technology

In recent years, research has been done to improve dermatoscopic technology. Polarimetric imaging techniques have been proposed to evaluate several optical properties in biological tissue, as well as imaging techniques to automate the ABCDE rule. Here are some examples of articles related to the research:

Lennart Jütte, Gaurav Sharma, Harshkumar Patel, and Bernhard Roth published an article in 2022 exploring the registration of polarimetric images for in vivo skin diagnostics.

They implemented a Mueller matrix polarimeter to register multiple feature-based images using both phantom and in vivo skin measurements. Their study emphasizes the challenges posed by patient movement during image acquisition, which can lead to misalignment and motion blur, affecting diagnostic accuracy. The research is particularly relevant to this thesis as it highlights the importance of improving the accuracy of polarimetric dermatoscopic analyses by accounting for possible patient movement during acquisition. [18]

In their article "Automating the ABCD Rule for Melanoma Detection: A Survey," Abder-Rahman H. Ali, Jingpeng Li, and Guang Yang (2020) provide a comprehensive review of methods aimed at automating the ABCD rule for melanoma detection. The authors highlight various approaches from the literature that address the subjective interpretation of these traits, offering objective evaluations through image processing and machine learning techniques. Their survey serves as a valuable reference for researchers interested in advancing automated tools for dermatological diagnostics. [19]

The article "Cognitive-Inspired and Computationally Intelligent Early Melanoma Detection Using Feature Analysis Techniques" (2023) focuses on developing methods for the early and reliable identification of melanomas. The research utilizes high-resolution images of skin lesions captured by advanced imaging equipment. Machine learning plays a crucial role in categorizing lesions and extracting highlighted features, addressing challenges such as uneven illumination through preprocessing techniques like histogram equalization and medial separation. The study introduces a novel image segmentation method called "Otsu" for lesion extraction and employs comprehensive dermoscopic evaluations, including the ABCD criteria (Asymmetry, Border, Color, and Dimension). [20]

These are some examples of the literature reviewed about the advances in dermatoscopic technology. In recent years the importance of better melanoma detection has become more relevant. There are some studies about the skin polarimetric advantages and some about automating the ABCDE rule using image processing and/or Machine learning. However, there is not currently a handheld device integrating an automated process to classify skin lesions through the ABCDE method and polarization features of diffusely reflected light. The device herein proposed is being developed to build a novel database and help physicians diagnose illness on a broader basis of information.

2.3 Intellectual property search

In order to ensure the feasibility of protecting the working principle of the developed prototype, a comprehensive search of intellectual property was carried out. In this regard, the World Intellectual Property Organization (WIPO) database was consulted using different keywords. In the following, those results related to our developed instrument are described.

CN106073719 - Multi-spectrum portable dermatoscope system: The application process to protect this invention was started in China in 2016. The device hardware consists in a liquid-crystal touch screen display, a imaging lens group that includes a circular-polarizing filter, a CMOS or CCD sensor array, and a multispectral light source comprising white, ultraviolet and near infrared LEDs. A software application controls lighting, focus adjustment, shooting and image processing through an interactive menu shown in the display. Additional buttons in the assembly case allows management of magnification and power on/off the device. Inventors claim that different light spectral ranges provide different information increasing accuracy of diagnosis. [21]

WO2022076792 - Smartphone-based Multispectral Dermascope: This application was promoted by the Wyant College of Optical Sciences in 2021. The invention consists in a low-cost handheld dermascope for detecting and diagnosing skin lesions based on polarized multispectral imaging (PMSI) and white light imaging (PWLI) implemented on a smartphone platform. Multispectral illumination is provided by different color LEDs (e. g., red, green and blue) arranged in a circular printed circuitboard (PCB) around either the built-in camera on the smartphone or the external one connected via a USB cable. A 3D-printed annulus serves as imaging guide having a length equal to the imaging optical system working distance. Polarization filters are positioned in front the light sources and camera. Two colorimetric algorithms are proposed to process collected dermal images. [22]

CN111640097 - Dermatoscope image recognition method and device: The application process to protect this invention was promoted by Shangai Yingtong Medical Technology CO., LTD. in 2023. The patent describes a method and device for dermatoscope image recognition. The method involves obtaining two dermatoscope images from the same person at different times during melanoma examinations, both containing the same target of

interest. A difference image is generated from these two images. The two dermatoscope images and the difference image are then processed using a machine learning model with two neural networks. The first neural network extracts features from the two dermatoscope images to produce a first recognition result and determines feature difference data during the extraction process. The second neural network uses the difference image and the feature difference data to obtain a second recognition result. Finally, the system determines whether the target of interest is melanoma based on the first and second recognition results. [23]

CN106108853 - Medical multispectral dermatoscope system: The system includes a dermatoscope and a host system designed as a single unit. The host system features a mobile stand (bogie), a main processing unit (host), and a display mounted at the top. The main unit is positioned on the stand, and the dermatoscope connects to it via cable. The dermatoscope has a front-end lens and a back-end handle, with the lens functioning as a multispectral light source. This system offers several advantages: it allows for switching between different spectral modes, which enables the comparison of skin lesion changes under various wavelengths. This capability improves the accuracy of identifying and diagnosing skin conditions. Additionally, the system can perform infrared thermal imaging on skin lesions, detecting temperature changes in the skin and surrounding tissues before any cellular changes occur. This early detection is crucial for diagnosing malignant tumors, skin infections, and other conditions, thus aiding in the timely diagnosis and treatment of tumors. [24]

CN106108853 - Multispectral local microscopic amplification 3D dermatoscope device: The device consists of a multispectral local microscopic amplification 3D dermatoscope device. The device features a lamp panel that integrates various types of lamp beads, including LED, UVA, cross-polarized light, and near-infrared. The amplification module is embedded at the image inlet of the device's housing, the reflector module is placed inside a cavity within the housing, and the 3D camera is located at the image outlet. The amplification module enlarge the image of the skin surface, while the reflector module captures this enlarged image and reflects it to the 3D camera. The image itself is composed of light emitted by the lamp panel and reflected off the skin surface. This device combines multi-

spectral imaging, magnification, and 3D imaging capabilities, allowing for comprehensive evaluation of skin conditions. It is particularly useful for assessing three-dimensional skin issues such as lumps, burns, irregularities, and subcutaneous blood vessels. [25]

Chapter 3

Methods

Like any engineering project, developing a physical device must begin with a solid theory and a good design. In the past, all designs were done by hand before developing the prototype physically. Nowadays, with all the technology we have at our disposal, we can use various design programs and simulation software. For example, for optical design, Oslo™ can be used, which can automatically calculate the optical characteristics, such as focal lengths. While for mechanical design we can use programs like Autocad™ or Solidworks™. These programs offer the advantage of being able to preview, what the physical prototype would look like visually, before having to spend resources building it physically.

3.1 Polarized light

Among the different characteristics of light, state of polarization (or simply, polarization) is often used as a probe to evaluate structural organization of matter. In the following, a brief introduction is presented to understand this statistical vector property of electromagnetic waves. Besides, a conventional technique to quantify it through measurement of intensities is described.

Let us assume a monochromatic beam of light with plane wavefront propagating in free space parallel to the z-axis in a Cartesian coordinate framework. In order to represent it mathematically, it is neccesary to define its electric/magnetic field amplitude, phase and state of polarization. However, Maxwell equations can be used to show that it is enough to

represent this optical beam with the electric field vector to study its propagation and interaction with matter. Besides, most of photodetectors are sensitive to electric field amplitude. Regarding the phase, it is related to the oscillation timing and location of the electric field vector within the wave. Considering a highly coherent beam of light, electric field vector can be projected in two orthogonal components with constant amplitude along $x-$ and $y-$axes. Also, it is found that phase difference between the $x-$ and $y-$components of the coherent wave can take stationary values between 0 and 2π. This phase difference and component amplitudes are crucial in determining the resulting state of polarization. State of polarization is the geometrical figure (conical section) drawn by the end of the electric field vector that can be identified when the optical wave propagates towards the observer. Consequently, polarization can be linear, circular or elliptical. In the two latter states, handedness is an additional feature to be identified. Then, the equation for a polarized electromagnetic wave is given as

$$\begin{aligned}\mathbf{E}(z,t) &= E_x(z,t)\hat{\mathbf{i}} + E_y(z,t)\hat{\mathbf{j}}, \\ &= E_{0x}\cos(kz-\omega t+\phi_x)\,\hat{\mathbf{i}} + E_{0y}\cos(kz-\omega t+\phi_y)\,\hat{\mathbf{j}}. \end{aligned} \tag{3.1}$$

- Linear polarization occurs when the phase difference $\Delta\phi = \phi_y - \phi_x$ is 0 or π, resulting in the electric field vector oscillating into a single plane. The plane subtends an angle with the $x-$axis given as $\arctan(E_{0y}/E_{0x})$.

- Circular polarization happens when the phase difference $\Delta\phi = \pm\frac{\pi}{2}$ and components amplitudes $E_{0x} = E_{0y}$, causing the electric field vector end to trace a circle. Sign implies the sense the circle is traced, namely, the handedness: clockwise (+) or counterclockwise (-). In the first case, light is known as right circularly polarized light and in the latter, left circularly polarized light.

- Elliptical polarization, a more general case, occurs when $\Delta\phi$, E_{0x} and E_{0y} assume any other arbitrary values, resulting in the electric field vector tracing an ellipse.

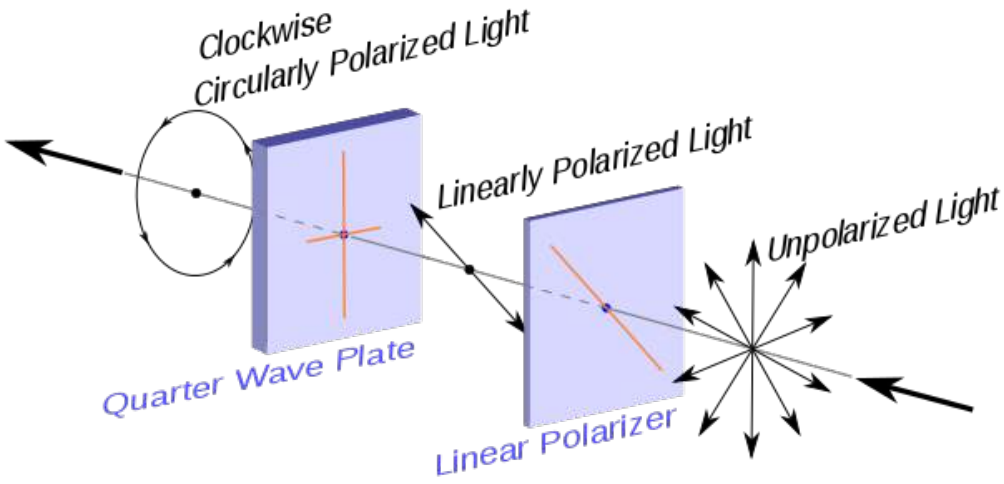

Figure 3.1 – Diagram representing a way to generate linear and circular polarized illumination. Source: WIkimedia Commons, Public domain.

3.1.1 Generation of linear and circular polarized illumination

State of polarization of light can be changed conveniently by its propagation through specific optical anisotropic components. For example, an unpolarized beam of light can be easily transformed to a linearly polarized light after the propagation through a dichroic polarizing film, which is a medium that extinguish the electric field component parallel to its absorption axis; these films are available commercially with different specifications being the extinction ratio the most relevant. For the purpose of this project, an achromatic linear polarizing film has been chosen so that absorbance varies little with the wavelength of the light source.

On the other hand, circularly polarized light can be generated by propagation of a linearly polarized beam of light through a birefringent optical element known as quarter-wave retardation plate. The fast-axis of the said retarder is oriented at 45° with respect to the incident linear polarization orientation angle. This setting divides the incident light into two orthogonal components with equal amplitude but propagating at different velocities. The phase difference therefore reaches a value of a quarter of a wavelength producing circularly polarized light. The selected retardation film to be used in the illumination LED source is also achromatic.

3.1.2 Stokes parameters: Definition and measurement

Formally, Stokes parameters results from the statistical analysis of an electromagnetic wave by the time autocorrelation and cross-correlation between the orthogonal linearly polarized components. This is, using definitions in Eq. (3.1),

$$s_0 = \langle E_x^* E_x \rangle + \langle E_y^* E_y \rangle , \tag{3.2}$$

$$s_1 = \langle E_x^* E_x \rangle - \langle E_y^* E_y \rangle , \tag{3.3}$$

$$s_2 = \langle E_x^* E_y \rangle + \langle E_y^* E_x \rangle , \tag{3.4}$$

$$s_3 = -i \left(\langle E_x^* E_y \rangle - \langle E_y^* E_x \rangle \right) , \tag{3.5}$$

where $\langle \cdots \rangle$ are for time average. It should be notice that autocorrelation gives the intensity of the field. Then, s_0 represents the total intensity of the analyzed light beam. s_1 provides the preference of the polarized beam to be linear horizontally polarized beam or vertically polarized beam. The following Stokes parameters are based on cross-correlations. s_2 gives the preference of the linearly polarized beam to be oriented at $+45^\circ$ or -45°. Finally, s_3 provides a measure of circularity of polarized light with right or left handdness.

There are a number of methodologies and modulation technologies to measure Stokes parameters.[26] Nonetheless, the rotating retarder Stokes polarimeter is often found in literature to analyze polarized light features. The matrix model to solve the inverse problem consist in measuring intensities transmitted through a system comprising a rotating quarter-wave retardation plate and a fixed linear polarizing plate. In order to derive the equation, Stokes-Mueller formalism is used. Then, it is written as

$$\mathbf{S}_o = \mathbf{P}(0^\circ)\, \mathbf{Q}(\theta)\, \mathbf{S}_i, \tag{3.6}$$

where

$$\mathbf{P}(0^\circ) = \frac{1}{2} \begin{pmatrix} 1 & 1 & 0 & 0 \\ 1 & 1 & 0 & 0 \\ 0 & 0 & 0 & 0 \\ 0 & 0 & 0 & 0 \end{pmatrix} \tag{3.7}$$

is the Mueller matrix for a linear polarizer with its transmission axis at 0°,

$$\mathbf{Q}(\theta) = \begin{pmatrix} 1 & 0 & 0 & 0 \\ 0 & \cos^2 2\theta & \sin 2\theta \cos 2\theta & \sin 2\theta \\ 0 & \sin 2\theta \cos 2\theta & \sin^2 2\theta & -\cos 2\theta \\ 0 & -\sin 2\theta & \cos 2\theta & 0 \end{pmatrix} \tag{3.8}$$

is the same for the quarter-wave retarder with its fast axis along θ, and $\mathbf{S}_i$ and $\mathbf{S}_o$ are the Stokes vectors for the incident and transmitted polarized light beam that are written as

$$\mathbf{S}_k = \begin{pmatrix} s_{0,k} \\ s_{1,k} \\ s_{2,k} \\ s_{3,k} \end{pmatrix} \tag{3.9}$$

where $k = \{i, o\}$. At the polarimeter output, the photodetector can measure only the intensity given by the first Stokes parameter $s_{0,o}$. Then, solving Eq. (3.6), it is found after an algebraic effort that the first row of $\mathbf{S}_o$ is

$$s_{0,o}(\theta) = \frac{1}{4}\left[2s_{0,i} + s_{1,i} + 2s_{3,i}\sin 2\theta + s_{2,i}\sin 4\theta + s_{1,i}\cos 4\theta\right], \tag{3.10}$$

which is a truncated Fourier series. Then, measuring transmitted intensities with the quarter-wave plate oriented at N-different θ angles with equidistant increments of $\Delta\theta$ to complete a full rotation, each coefficient is calculated by using discrete Fourier analysis. Thus,

$$A = \frac{1}{N}\sum_{n=0}^{N-1} s_{0,o}(n\Delta\theta) = \frac{1}{4}\left(2s_{0,i} + s_{1,i}\right), \tag{3.11}$$

$$B = \frac{2}{N}\sum_{n=0}^{N-1} s_{0,o}(n\Delta\theta)\sin 2n\Delta\theta = \frac{1}{2}s_{3,i}, \tag{3.12}$$

$$C = \frac{2}{N}\sum_{n=0}^{N-1} s_{0,o}(n\Delta\theta)\sin 4n\Delta\theta = \frac{1}{4}s_{2,i}, \tag{3.13}$$

$$D = \frac{2}{N}\sum_{n=0}^{N-1} s_{0,o}(n\Delta\theta)\cos 4n\Delta\theta = \frac{1}{4}s_{1,i}. \tag{3.14}$$

Solving the previous equation system allows to retrieve the Stokes parameters (state of polarization) of the incident polarized beam. That is to say,

$$s_{0,i} = 2(A - D), \tag{3.15}$$

$$s_{1,i} = 4D, \tag{3.16}$$

$$s_{2,i} = 4C, \tag{3.17}$$

$$s_{3,i} = 2B. \tag{3.18}$$

3.1.3 Stokes imaging polarimetry

Polarimetric bioimaging is based on analyzing intensity images obtained with diffusely reflected light from a biological specimen surface using a polarized light source. Then, because of light scattering, it is expected that correlation between orthogonal electric field components decreases, which affects coherence and polarization degrees. In particular, the used imaging polarimetry technique is based on a rotating quarter-wave retardation plate to generate a θ-stack of intensity images, where θ is the fast-axis orientation angle. As previously described, Fourier analysis is applied at each pixel through the entire stack, resulting the truncated series coefficients that are combined adequately to obtain the Stokes parameters: s_0, s_1, s_2, and s_3. Furthermore, additional polarization features are calculated, such as Degree of Polarization (DoP), Degree of Linear Polarization (DoLP) and Degree of Circular Polarization (DoCP), and Angle of Lineal Polarization (AoLP), which are given as [26]:

$$DoP = \frac{\sqrt{s_1^2 + s_2^2 + s_3^2}}{s_0} \tag{3.19}$$

$$DoLP = \frac{\sqrt{s_1^2 + s_2^2}}{s_0} \tag{3.20}$$

$$DoCP = \frac{s_3}{s_0} \tag{3.21}$$

$$AoLP = \frac{1}{2}\arctan\frac{s_2}{s_1} \tag{3.22}$$

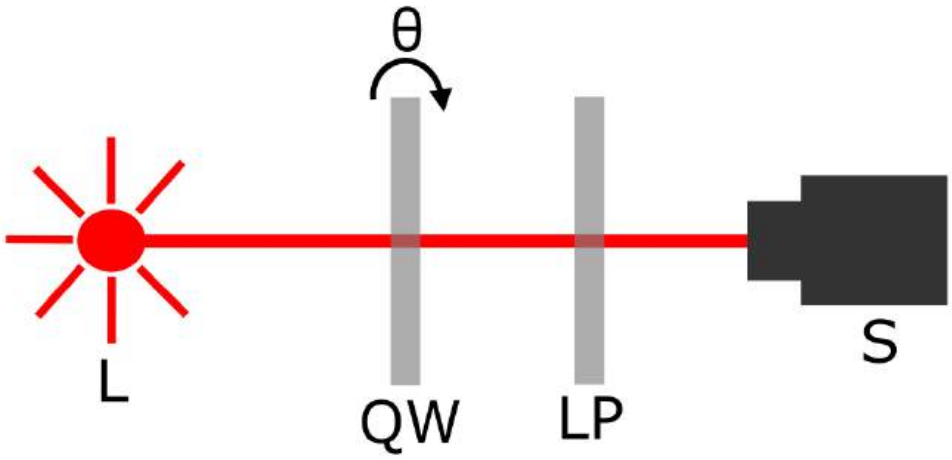

Figure 3.2 – Diagram representing the Stokes polarimeter used in this study. L represents the diffused reflected light, while QW and LP are the quarter-wave plate and linear polarizer respectively and S is the sensor.

3.2 Interactions between skin and light

Studying the interaction between skin and light will help us discover new methods of skin analysis, such as capturing images at different depths or observing invisible elements to the naked eye.

In the skin, three basic layers are identified [27]:

- Stratum corneum of thickness 0.01–0.02 mm
- Epidermis of thickness 0.04–0.15 mm
- Dermis of thickness 1–4 mm.

The stratum corneum, which is the upper layer of the skin, has a refractive index relative to air of about 1.5. The epidermis consists of tissue-bases that absorb and scatter light and an absorbing component, melanin. The dermis consists of the same tissue basis in which, blood vessels, capillaries, are evenly and randomly distributed. [27]

The light interacts with the skin in four different ways: absorption, reflection, transmission and scattering.

Color	Wavelenght	Penetration depth
Red	625–740 nm	4-5mm
Green	500–565 nm	2-3mm
Blue	440–485 nm	<1mm

Table 3.1 – Penetration Depth of Different Light Wavelengths in Skin. Data obtained from: Caerwyn A. (2017) [28]

- Absorption: The light absorption in the skin depends on the chromophores, with melanin being the most relevant.
- Reflection: This is a natural phenomenon caused by the differences in the refractive index of the skin and the air.
- Transmission: When light reaches the skin at a near-normal angle, about ninety-five percent of it is transmitted to the deeper layers, whereas only five percent is reflected in the stratum corneum.
- Scattering: When light enters the skin, it is deflected in multiple directions as it passes through the skin because of the microscopic irregularities and structures within the tissues, such as collagen fibers, cells, and other microscopic structures. Polarized light can be used to precisely determine scattering and give more information about the structures of the tissue.

3.2.1 Penetration Depth of Different Light Wavelengths in Skin

It is known that light is an electromagnetic wave, and that each specific wavelength corresponds to a different color. When the skin is illuminated using different wavelengths, each wavelength penetrates the skin at different depths. Thus, if an image of the skin is taken with varying wavelengths, images of different depths can be achieved.

Table 3.1 shows the penetration depth of different wavelengths of light in the skin. This means that if the skin is illuminated by blue light, a superficial image is obtained, whereas using red light results in a deeper image. This way, using RGB LED illumination for the device provides the opportunity to take photos of three different layers of the skin, in

addition to the white light photo.

3.2.2 Use of Green Light for Vein Visualization

The main advantage of using green light (500-565 nm) is its unique interaction with the red pigmentation of blood caused by hemoglobin. Green light is best absorbed by red, resulting in a great contrast with other tissues when a photo is taken with green illumination. This interaction is the reason behind the sensors on smartwatches, which use a green LED to detect heart rate and other parameters.

3.3 Image processing for ABCDE rule

3.3.1 Image preparation

Before attempting to process the image to extract the ABCDE parameters, it is necessary to first preprocess it to remove as much noise as possible, leaving only the desired features of the image, which in this case would be the mole and the skin. Since hair can affect the processing, it is digitally removed first. A morphological filter is used for this purpose, which extracts only the small structures from the image, in this case, the hair. In this way, the hair can be automatically selected and removed, leaving only the skin and the mole. The morphological filter that was chosen to implement is the "Top-Hat" filter, which successfully removed the hair from many images without affecting the rest of the original image. [29] It should be pointed out that more advanced techniques can be implemented to preprocess the skin lesion images. [30]

3.3.2 Automatic ABCDE extraction

There are several ways to digitally extract the ABCD parameters of a mole quantitatively. In fact, there is an article that compiles various methods from which algorithms can be built on a computer to obtain these parameters [19]. For this project, the methods with the lowest error percentage and that were also easy to implement in Python were selected, and for each parameter, an algorithm was developed.

3.3.2.1 Asymmetry

The first step to calculate the symmetry of the mole is to obtain its edge. This is done very simply by binarizing the image and using a specific library in Python capable of extracting the perimeter of any binarized image. Subsequently, two axes of symmetry of the mole are obtained. To do this, the centroid of the image is first determined. For the centroid of a binary image, the moments of the image are first calculated using `cv2.moments`. The coordinates of the centroid are obtained from the spatial moments of the first and zero order, given by the following equations:

$$cX = \frac{M_{10}}{M_{00}}$$

$$cY = \frac{M_{01}}{M_{00}}$$

Once the centroid is obtained, the two axes of symmetry can be easily drawn. These are lines that pass through the centroid and touch the two ends of the perimeter of the mole. After obtaining the axes of symmetry and the border of the mole, the asymmetry of the mole can be mathematically calculated. The two sides of the axis of symmetry are subtracted, and the resulting area from the difference between them is obtained, as shown in the figure 3.3. Once this area and the total area of the mole are obtained, the asymmetry index is calculated using the following equation:

$$\text{Asymmetry Index} = \frac{\Delta A}{A_T} \times 100\%$$

Finally, the two asymmetry indices obtained with the two different axes of symmetry are averaged.

3.3.2.2 Border

Once the edge of the mole is extracted, the perimeter and area of the mole in pixels can be calculated. With this information, the irregularity of the mole can be calculated using the following equation:

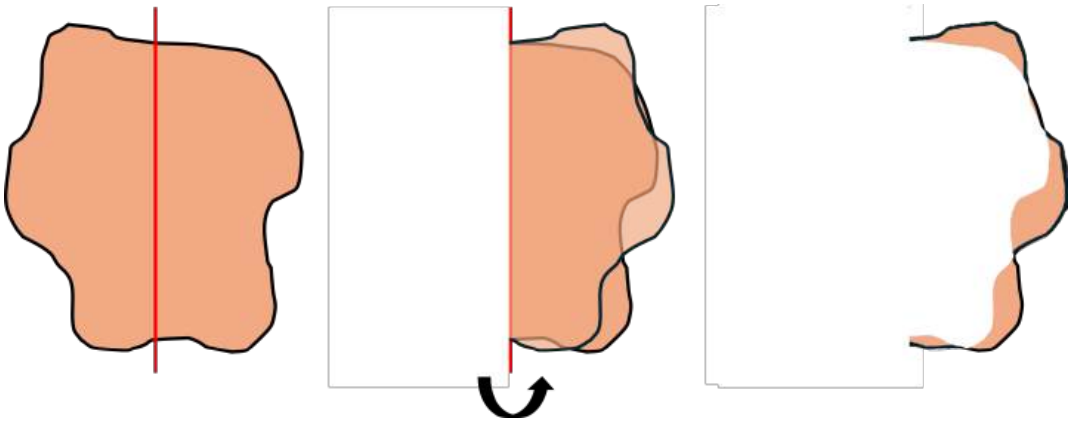

Figure 3.3 – Diagram illustrating the process by which the asymmetry of the mole is obtained from the axis of symmetry.

$$\text{Irregularity} = \frac{p^2}{4\pi A}$$

3.3.2.3 Color variegation

To obtain the color parameter, first, the color palette corresponding to the mole is extracted using the `Pylette` library in Python. This provides the values from 0 to 255 corresponding to the different shades of gray of the mole. With these values, the following equation is used to obtain a percentage of color variation:

$$\text{Color variegation index} = \frac{C_{max} - C_{min}}{256} \times 100\%$$

3.3.2.4 Diameter

The diameter is obtained from the largest symmetry axis by calculating its real dimensions, considering that 1200 pixels are equivalent to 6 mm.

3.3.2.5 Evolution

Finally, to obtain the mole's evolution, all data obtained from the other parameters are saved in a specific folder. This way, a record is maintained for future reference.

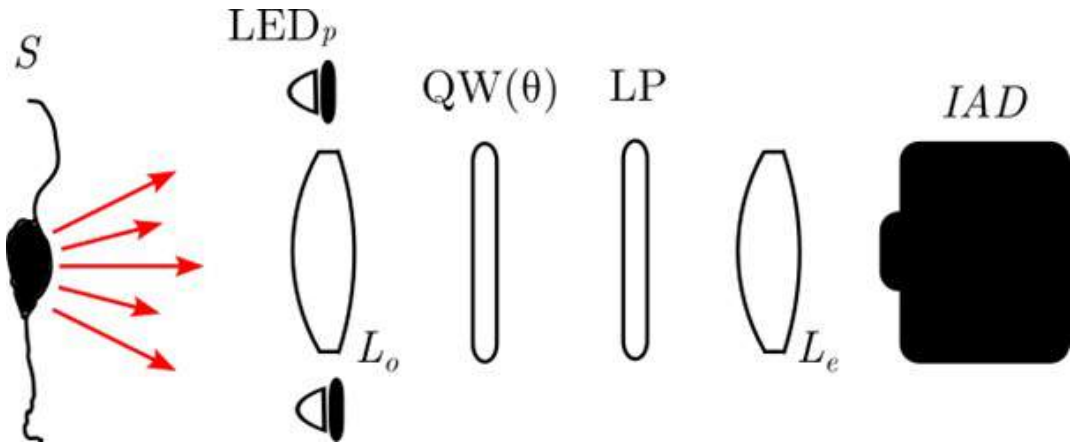

Figure 3.4 – Scheme representing the working principle of Stokes imaging polarimetric dermatoscope. IAD: Image (Intensity) Acquisition Device, Lo,e: Objective and eyepiece lenses, LP: Linear polarizer, QW(θ): Rotating quarter-wave plate, LEDp: Polarized LED source, S: Sample.

3.4 Optical design

The device comprises an illumination source, an image-forming optical system, the Stokes polarimeter, and the sensor. Figure (3.4) shows a diagram of the core elements of the device. Each element is explained below.

3.4.1 Illumination source

The illumination source consists of an addressable RGB LED ring lamp covered by achromatic polarizing and quarter-wave retardation films. This configuration ensures the production of a uniformly circularly polarized illumination spot on the analyzed skin lesion. It also features an interchangeable cone, designed to serve four purposes:

- First, to prevent involuntary movements of the analyzed skin during image acquisition.
- Second, to ensure that the skin is exactly in focus, neither too close nor too far away.
- Third, to concentrate the light and prevent external light from interfering with the analysis.

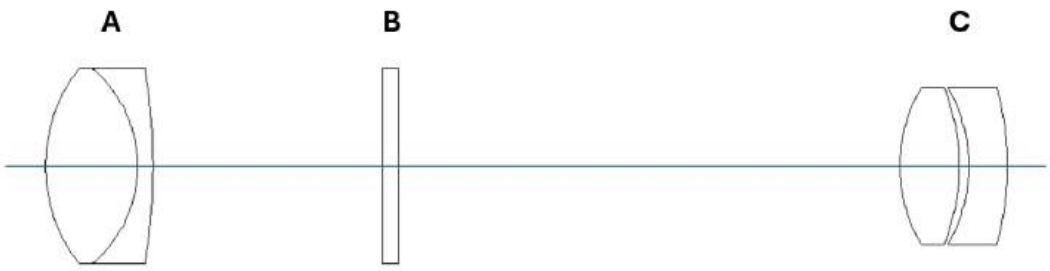

Figure 3.5 – Diagram representing the optical system simulated in Oslo. A and C represent the doublet lenses, while B is the polarizing element incorporated into the system. The wave retarder could not be included due to software restrictions.

- Fourth, the cone has a polarizing film built-in, meaning that the polarizing light can be easily changed between circular and linear, for research purposes.

3.4.2 Image-forming optical system

The main objective of this design was to create an achromatic image-forming system free from aberrations while considering the polarizing elements that it would incorporate. The Petzval objective design was chosen, shown in figure (3.5), which consists of a total of four lenses arranged in two doublets, an objective and an eyepiece. This design offers the advantages of being achromatic, with a short focal length and low magnification. The only notable disadvantage is its limited depth of field, which was corrected using a diaphragm. Interestingly, the Petzval lens construction is typically utilized for handheld thermal imaging applications with short to medium focal lengths. The diaphragm was added later to obtain a larger field of view and to reduce possible optical aberration, shown in figure (3.6).

3.4.3 Stokes polarimeter

Diffusely reflected light is gathered by an objective lens and passed through a Stokes polarimetric setup, which includes a rotating quarter-wave plate and a linear polarizer, both achromatic.

These two elements are placed between the lenses and the quarter-wave plate is rotated by a stepper motor, completely in sync with the sensor and the illumination ring. Finally,

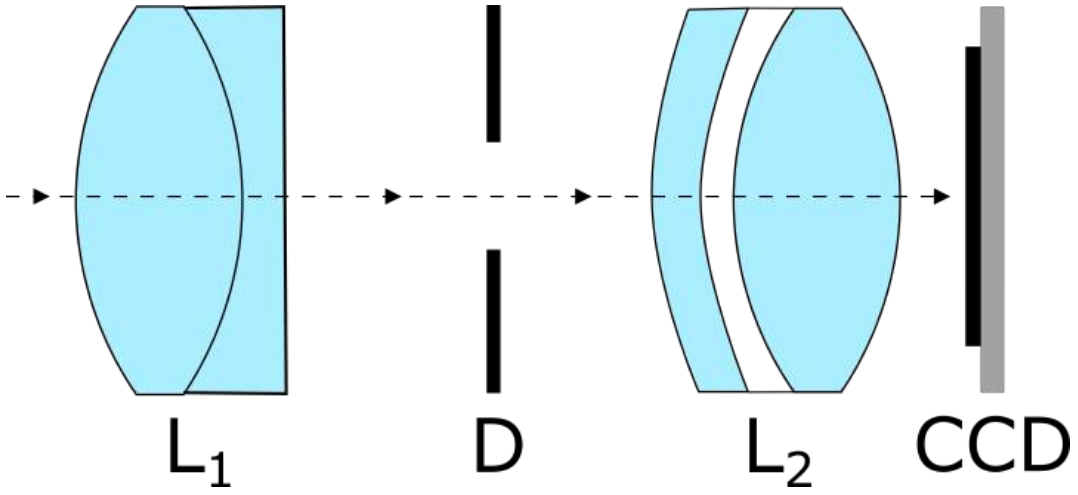

Figure 3.6 – Diagram representing the inclusion of the diaphragm in the system.

the spatially modulated intensity light field is collected by an eyepiece lens and digitized by a monochromatic CMOS sensor, which has a resolution of 1920x1200 pixels.

The stack depth defined to calculate the Stokes parameters consists of thirty-six images, Less than that could decrease processing time but at the cost of getting worse results, and more images could mean longer processing and acquisition time. Also, thirty-six is a very convenient number, because completing the full rotation means movements of exactly 10° and the results obtained were pretty good.

3.4.3.1 Rotating element

The minimum number of images required to obtain the Stokes parameters is eight. However, as the number of images increases, the quality of the results also improves, but so does the capturing and processing time. Thirty-six images per wavelength were chosen for three reasons: first, it provides enough images to obtain high-quality results; second, this number of images is manageable for most computers, without significantly increasing processing time or occupying too much disk space; third, it is a divisible number of 360 (the full rotation), which facilitates both the physical design and the coding.

Two different mechanisms were considered for transferring the motion from the motor to the waveplate: gears and bands. The advantages and disadvantages of each are shown in Table 3.2. Considering these factors, the band was chosen due to its easier implementation.

The main disadvantage of slight inaccuracy was resolved by designing and implementing a ring with thirty-six holes, each at 10°, and a U-shaped sensor, giving feedback to the microcontroller and converting it into a closed-loop mechatronic system.

Mechanism	Advantages	Disadvantages
Gears	• High torque transmission efficiency. • Precise and consistent movement. • Long lifespan with minimal maintenance.	• Potential for backlash, leading to slight inaccuracies. • Requires precise alignment and can be difficult to assemble. • Can be noisy during operation.
Band	• Smooth and quiet operation. • Easier to set up and align compared to gears. • Absorbs vibrations and shocks, protecting the system.	• Potential for slippage, leading to reduced accuracy. • Generally lower torque transmission compared to gears. • Bands can wear out and need replacement more frequently.

Table 3.2 – Advantages and disadvantages of gears and band mechanisms

3.4.4 Sensor

The sensor used for capturing images is a monochromatic 8-bit CMOS. With a total resolution of 1920x1200 pixels, Each image taken is automatically cropped to 1200x1200 pixels, with the purpose of obtaining square images of 6x6mm of the skin and also getting rid of the possible vignetting. The sample and CMOS sensor planes are conjugated.

All image acquisition settings ensure an unsaturated and focused image of the skin region of interest. The system can be configured to capture a white light picture of the region of interest with the aim of applying an automated ABCDE process to classify the nevus. Also, RGB LEDs can be individually activated to execute the polarimetric process

that requires the rotation of the quarter-wave plate synchronized with the frame acquisition to build a databox. Each image is taken with an exposure time of 7 ms, to ensure high-quality polarization features retrieved without compromising processing time.

The device captures a total of one hundred and nine images each time, which consists of thirty-six of each Red, Green, and Blue color, and one with white illumination.

3.5 Code

The code used was developed exclusively for this project. It performs the acquisition and processing of images to obtain the Stokes parameters and degrees of polarization, as well as the process for lesion classification through the ABCDE method. The code is written in Python, as it is an excellent programming language for image processing, with many libraries available for machine learning and image processing, and it has the advantage of being free software, without the need to obtain a license like other programming languages or environments such as Matlab or LabView. The acquisition time for all the images takes sixty-four seconds, and the processing time to obtain both the polarimetric parameters and ABCDE values takes approximately three hundred seconds. This means that the entire process takes less than ten minutes.

3.6 Prototype development

3.6.1 Prototype modelling

Solidworks was used to design and visualize all the components for the device. It provided an excellent way of making a digital 3D model, in which all the exact measurements and distances were contemplated. The design for the interior of the device is shown in figure (3.7), This visualization also helped to get a first idea of how the final prototype would be, and to choose the best materials for each element of the device.

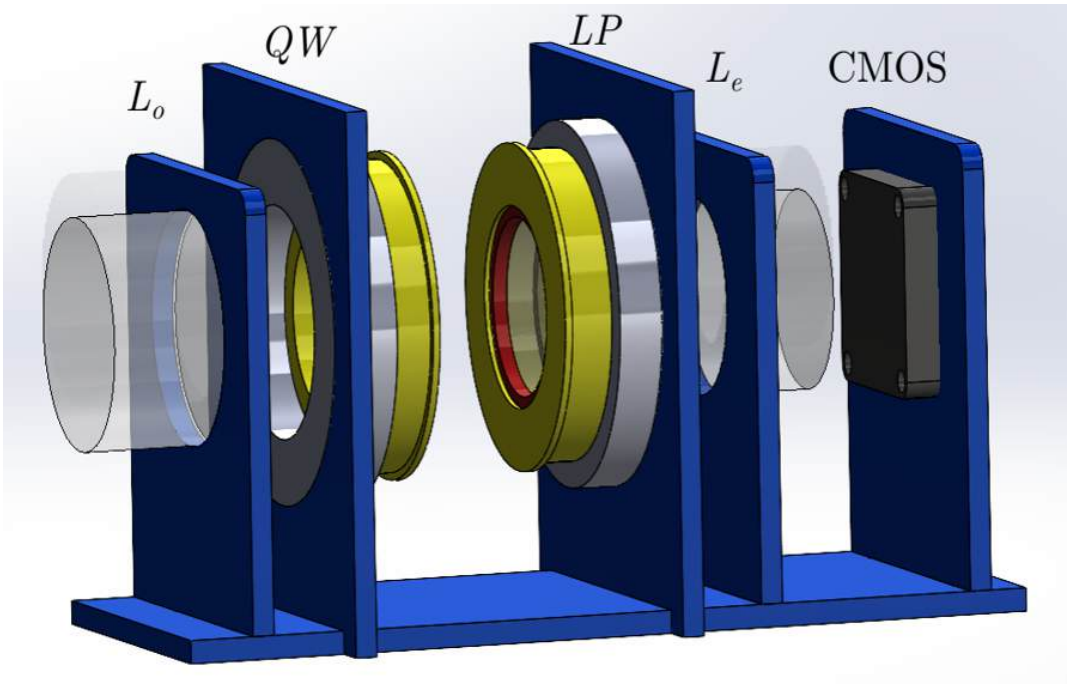

Figure 3.7 – Design made in SolidWorks, which contemplates all the optics and exact distances between each component.

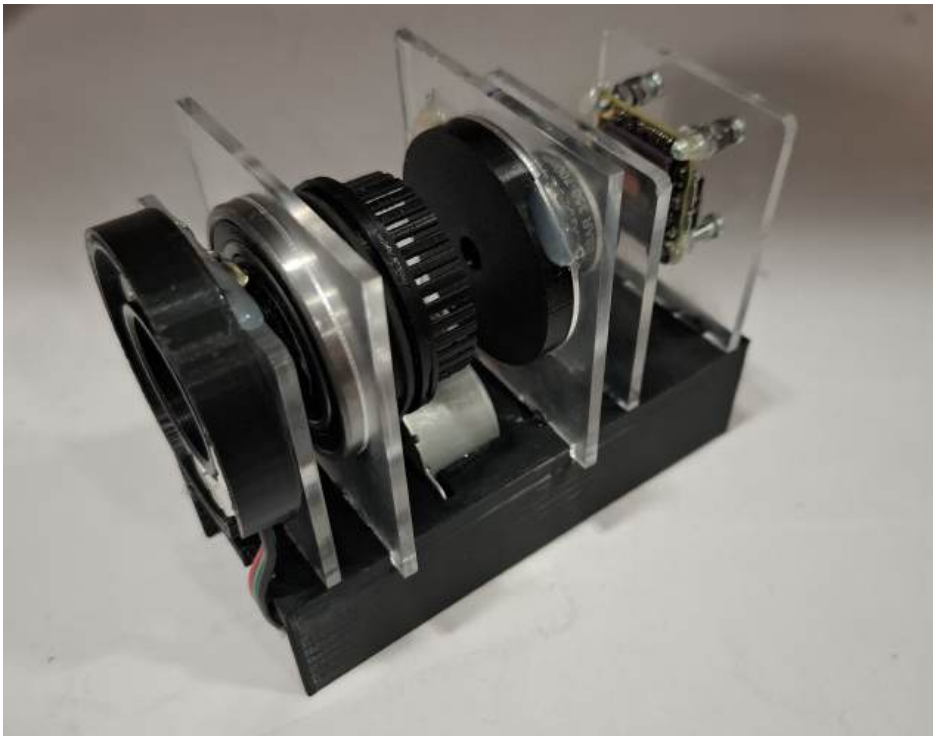

Figure 3.8 – The completed system includes all improvements, including the notched ring for the sensor to measure the angular rotation and the diaphragm.

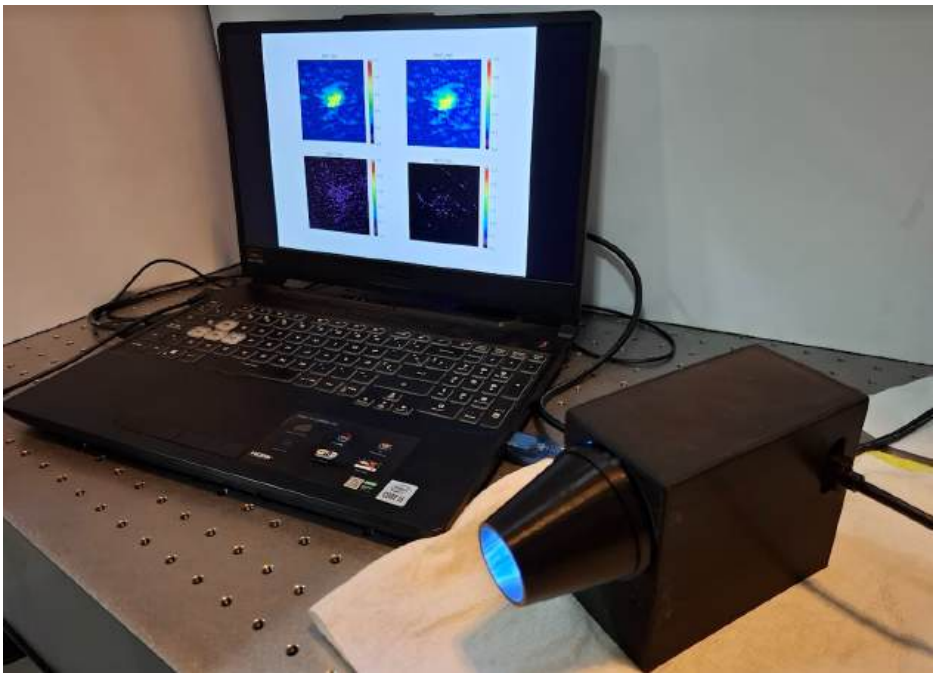

Figure 3.9 – Image of the completed and functioning device; it only needs to be connected to a computer to operate.

3.6.2 Prototype fabrication

Nowadays, there are several ways to build a physical prototype, including CNC machining, 3D printing, and vacuum casting, each with its own characteristics, advantages, and disadvantages. For the development of this device, after considering several options and materials, a combination of 3D printing and acrylic laser cutting was chosen. 3D printing offers the main advantage of being an extremely fast and accurate option, allowing the opportunity to test different filament materials. Acrylic was chosen because it provides good structural integrity and is visually very appealing in combination with the black PLA filament used in the 3D printer.

Each piece was carefully designed and printed, using minimal tolerances. In figure 3.8 the interior of the device is shown, which includes all functioning parts. In figure 3.9 the final device working is shown, with a polarimetric analysis in the background. The device is connected directly to the computer, and the Python program developed handles everything, from image acquisition to processing.

The image acquisition time is 64 seconds and the image processing time is about 270

Figure 3.10 – Final assembly, includes the ergonomic handle. Ready to use.

seconds. This means that the entire analysis takes less than ten minutes to complete, with the results displayed and saved.

The device is intended to be handheld, so an ergonomic handle was added, which completed the final design. The fully functional model is shown in Figure3.10.

An important thing to note is that the device only needs a laptop or computer to function; it does not require any external hardware or a power bank, as it receives all the electrical energy directly from the USB port, which also serves as a communication cable between the computer and the microcontroller. The computer does not need to be a powerful one; the program developed is capable of running smoothly on most commercial computers, only requiring Windows 8+ for the drivers and USB 3.0 for communication with the sensor and microcontroller.. Additionally, since Python is free software, this makes the device highly accessible for most physicians.

Finally, the device has a very ergonomical design for both the physician and the patient. It is lightweight, relatively compact, and features an ergonomic handle. Additionally, it includes a cone that helps to maintain the skin in place during the acquisition time, making

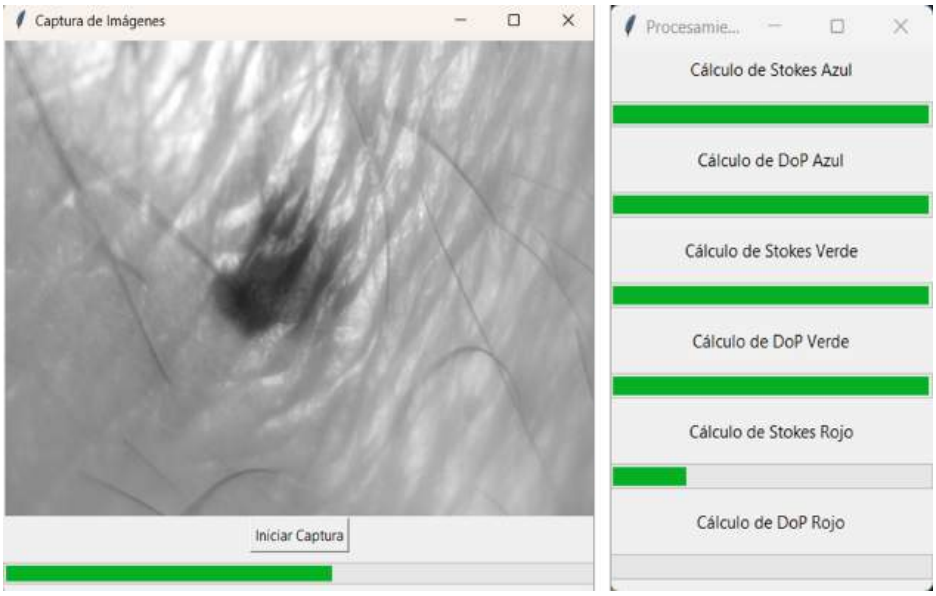

Figure 3.11 – User Interface

it more comfortable for the patient.

For a simpler user experience, an application was developed from the Python program. This application can run on any computer with Windows 8 or later and has a fairly straightforward user interface, as shown in Figure 3.11. First, a live video of what the camera is capturing is displayed so the doctor can properly position the device and center the mole in the image. Once positioned correctly, the doctor only needs to click the "Start Capture" button. Doing so will display a progress bar indicating how much time is remaining to capture all the images. After all images have been captured, the dermatoscope can be removed, and another window will appear showing six progress bars that indicate the status of the processing of all images and the extraction of both the Stokes parameters and the degrees of polarization for each wavelength. Once this processing is complete, all windows automatically close, and the result windows open, displaying the four Stokes parameters for each wavelength, the degrees of polarization for each wavelength, and the image taken with white illumination.

Chapter 4

Results

4.1 Calibration of the Stokes polarimetry module

In order to guarantee the accurate retrieving of Stokes parameters, the polarimetric module was tested using a commercial Stokes polarimeter as a reference. To ensure that all components were correctly aligned, including the polarizing filters of the illumination system:

- The linear polarizer and the wave plate must be aligned at 0°.
- The two films of the circular polarizer used in the illumination system must be perfectly aligned to ensure proper circular polarization.
- The linear polarizer used in the illumination system must be oriented at 45°.

Maximum and minimum values of irradiance diffusely reflected by a surface and reaching the detection plane were obtained illuminating an spectral white reference target [31] and blocking the incident light completely, respectively. These two values were used in to obtain the Stokes parameters.

4.2 Testing imaging system

The first test of the device was to check if it had any kind of optical aberrations, focusing on vignetting and distortion, which were the most notorious aberrations of the predecessor

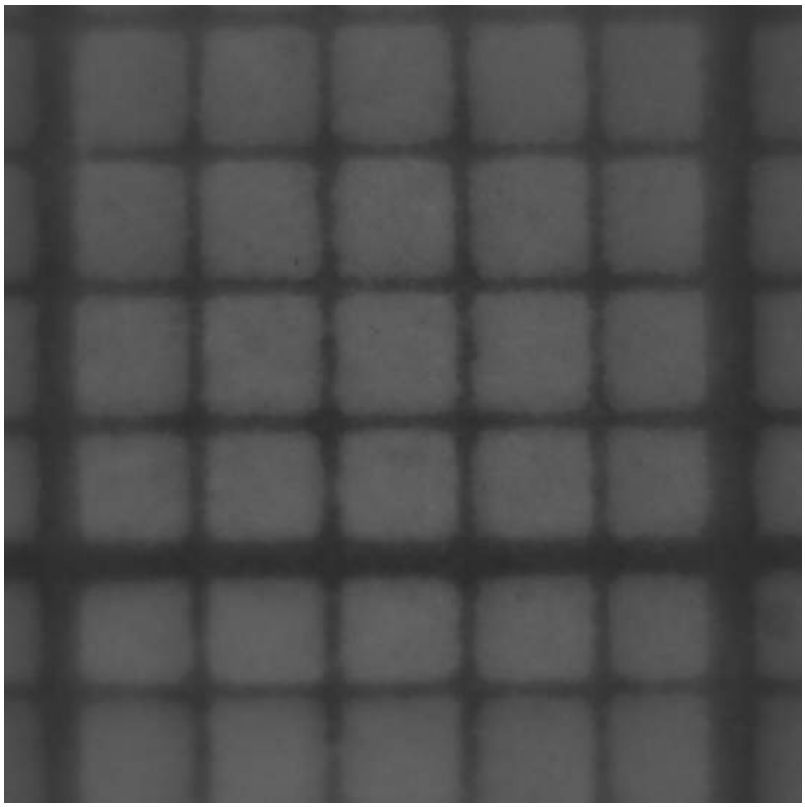

Figure 4.1 – Photograph of a millimeter graph paper.

device. To test these aberrations, a millimeter sheet was used. The image is shown in Figure 4.1. To check for distortion, the lines are perfectly straight, indicating that there is no visible distortion. As for vignetting, the intensity of the pixels seems perfectly homogeneous from the center to the edges, meaning that the optical system does not produce visible vignetting.

To test the device in a real application, a healthy mole was analysed. The first analysis used white illumination, testing both linearly and circularly polarized light. These images are shown in Figure 4.2. It is the same mole, and the device maintained the exact same configuration parameters for both photos, only changing the type of polarization used. It is notable that the linearly polarized light produced a brighter image, whereas the circularly polarized light resulted in a slightly darker image. The reason for this difference is that the first layer of the skin reflects linearly polarized light more easily, and this reflection reaches the sensor, producing a brighter image. This is the main notable difference between the two types of illumination. This difference does not significantly affect the ABCDE classification, but it will impact the extraction of the Degree of Polarization (DoP).

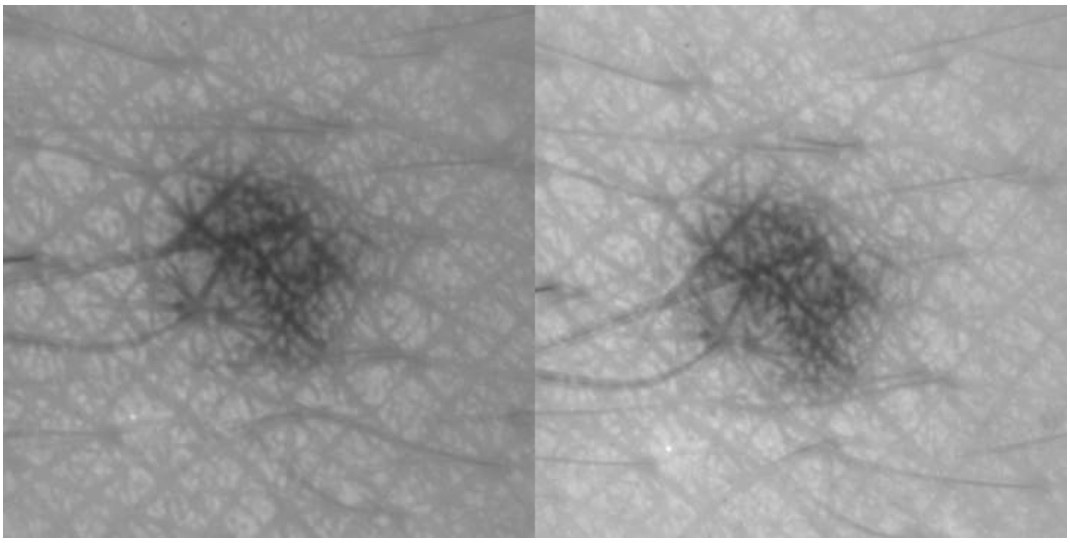

Figure 4.2 – Photographs of a mole illuminated with white light: circularly polarized illumination on the left and linearly polarized illumination at 45 degrees on the right.

The result of the analysis in Oslo is shown in figure (4.3), it can be observed that there is no chromatic aberration and that the optical aberrations caused by the system are extremely small. This is reflected in the tests taken with the millimeter paper and generally in the photographs taken of the skin.

4.3 Comparison between circularly a linearly polarized illumination.

The Stokes parameters extracted from the mole using circularly polarized illumination are shown in figures 4.4 (blue light), 4.5 (green light), and 4.6 (red light). The Stokes parameters extracted from the mole using linearly polarized illumination are shown in figures 4.10 (blue light), 4.11 (green light), and 4.12 (red light).

The Degrees of polarization (DoP, DoCP and DoLP) are also automatically calculated and displayed, as well as the Angle od Polarization (AoP). These images are shown in figures 4.7 (blue light), 4.8 (green light), and 4.9 (red light) for circular polarized illumination. And figures 4.13 (blue light), 4.14 (green light), and 4.15 (red light) for linearly polarized light at 45°

The device successfully calculated the Stokes parameters and subsequently used these

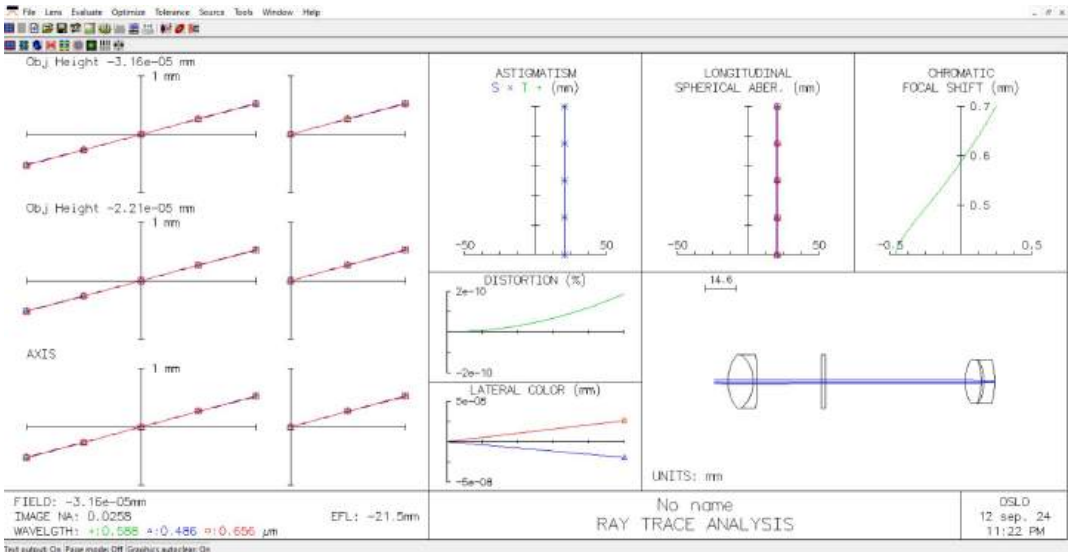

Figure 4.3 – Oslo ray trace analysis.

parameters to calculate the degrees of polarization. To test the two types of polarization, two cones with different filters were used: the first with a linear polarizer oriented at 45° relative to the other components, while the other cone had a circular polarizer. Comparing both results, it can be concluded that the circular polarizer is more efficient at eliminating surface reflection of the skin, allowing for clearer images at different skin depths. This is because when linearly polarized light is used, part of this light reflects off the skin surface, meaning it does not penetrate. Consequently, the resulting image is a superposition of the surface skin image with the deeper surface image.

The four Stokes parameters alone do not provide useful information for the doctor. However, when the degrees of polarization are obtained, an image can be observed in which the different tissues and cells in the skin that change the polarization state of the incident light. This highlights the accumulation of melanocytes in the mole, providing more information about the behavior of the mole with respect to its depth. Additionally, the collagen structures of the skin can be observed, as they also have the ability to modify the polarization state of the light, although this information is not particularly relevant for the study of melanomas.

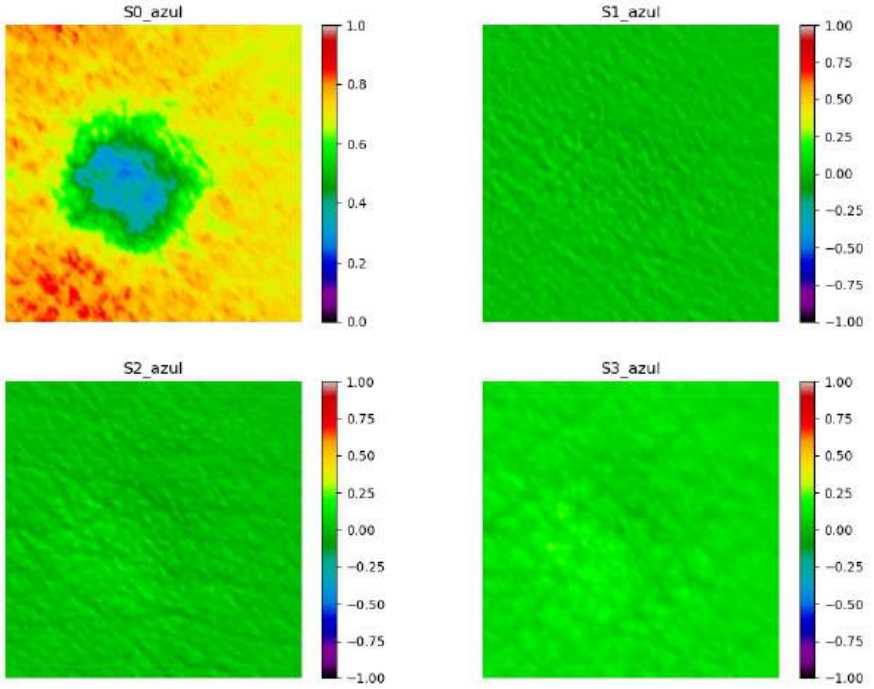

Figure 4.4 – Stokes parameters with circularly polarized blue light.

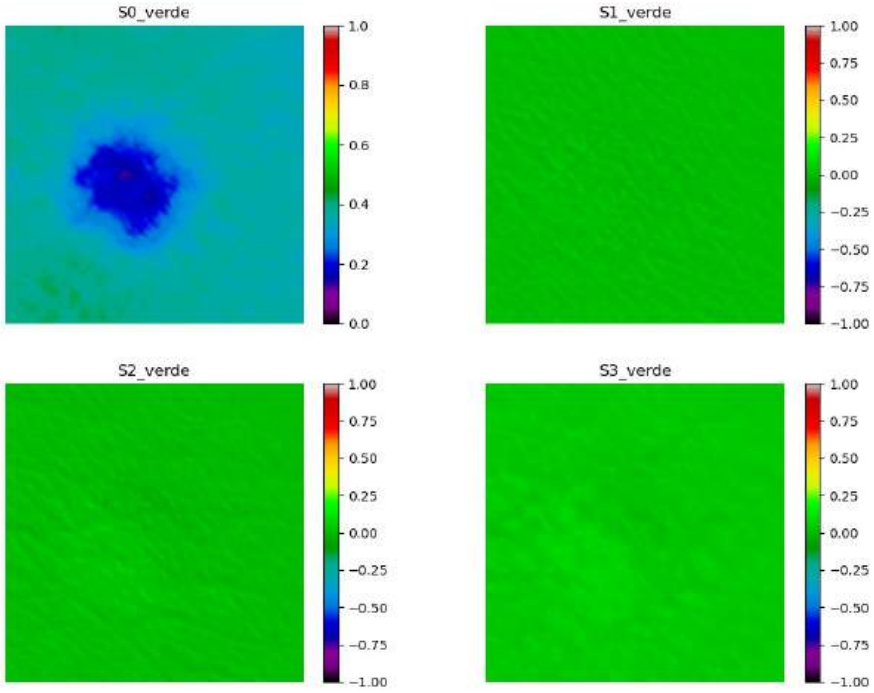

Figure 4.5 – Stokes parameters with circularly polarized green light.

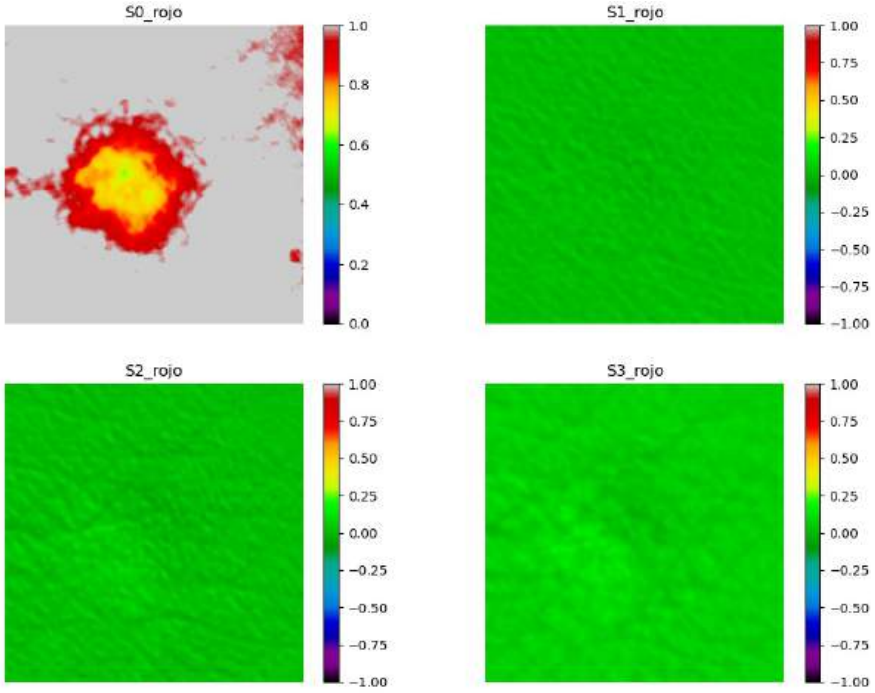

Figure 4.6 – Stokes parameters with circularly polarized red light.

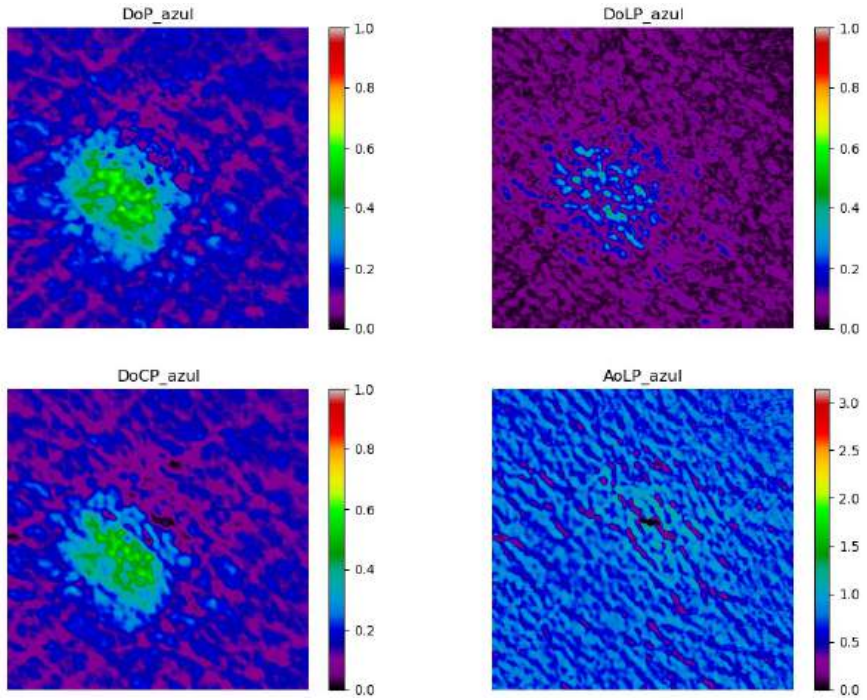

Figure 4.7 – Degree of Polarization (DoP), Degree of Linear Polarization (DoLP), Degree of Circular Polarization (DoCP), and Angle of Linear Polarization (AoLP) with circularly polarized blue light.

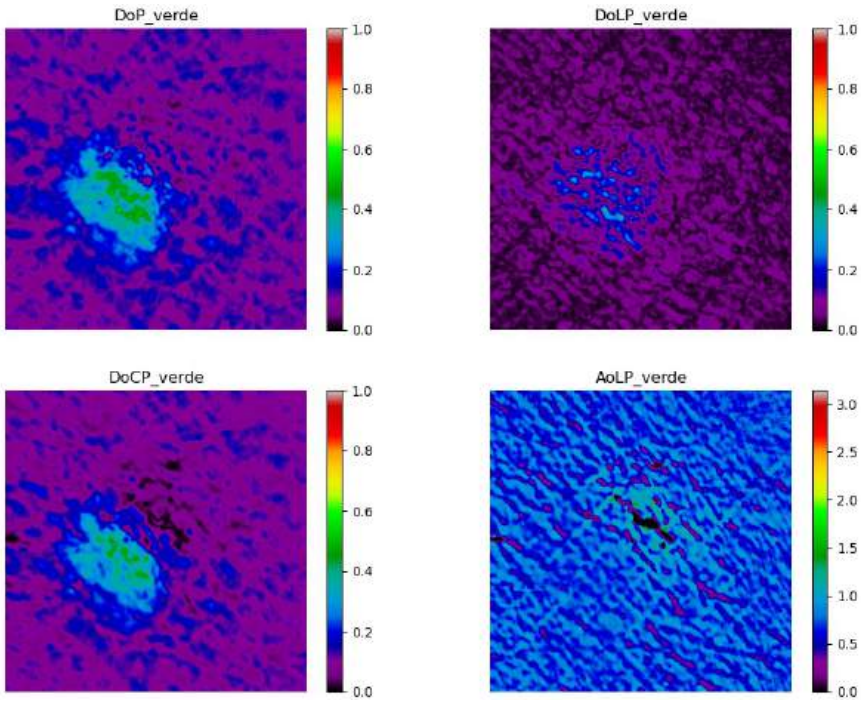

Figure 4.8 – Degree of Polarization (DoP), Degree of Linear Polarization (DoLP), Degree of Circular Polarization (DoCP), and Angle of Linear Polarization (AoLP) with circularly polarized green light.

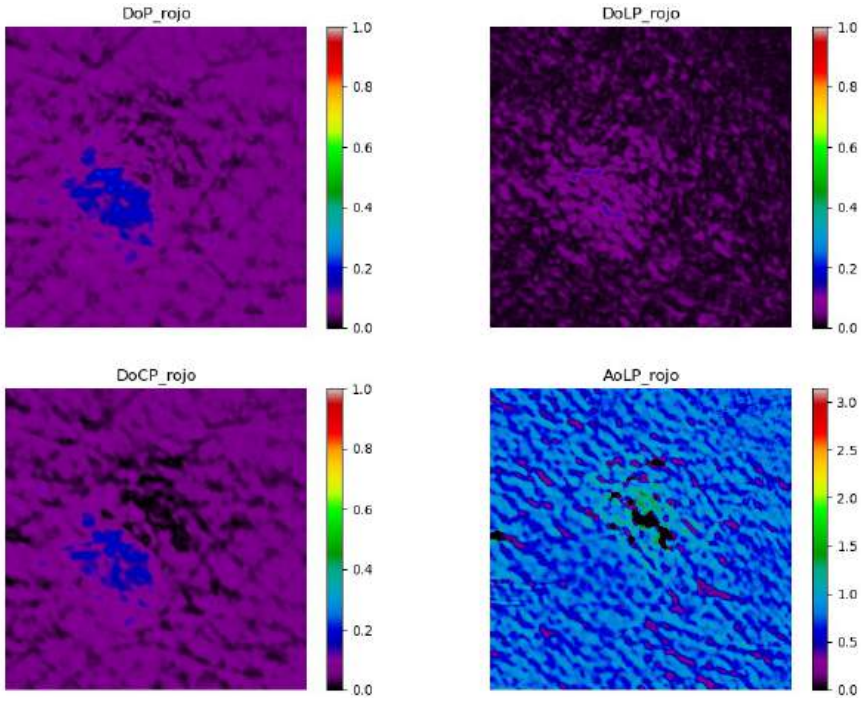

Figure 4.9 – Degree of Polarization (DoP), Degree of Linear Polarization (DoLP), Degree of Circular Polarization (DoCP), and Angle of Linear Polarization (AoLP) with circularly polarized red light.

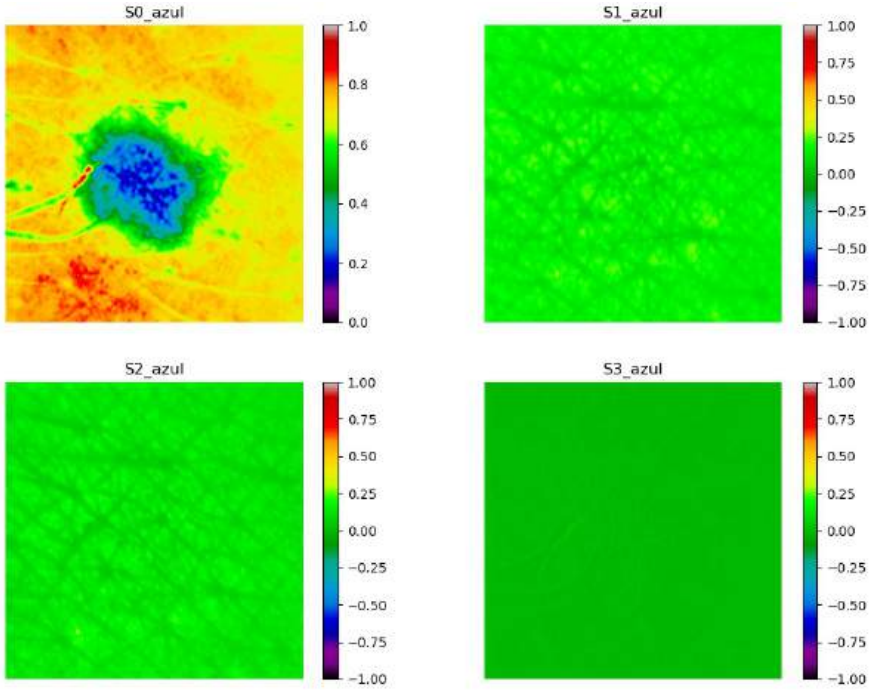

Figure 4.10 – Stokes parameters with linearly polarized blue light at 45 degrees.

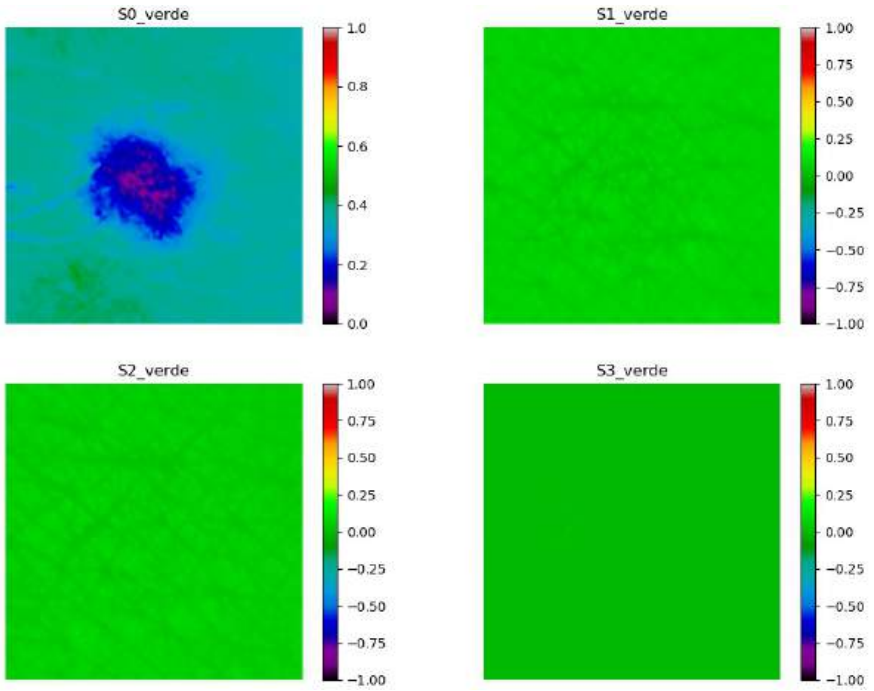

Figure 4.11 – Stokes parameters with linearly polarized green light at 45 degrees.

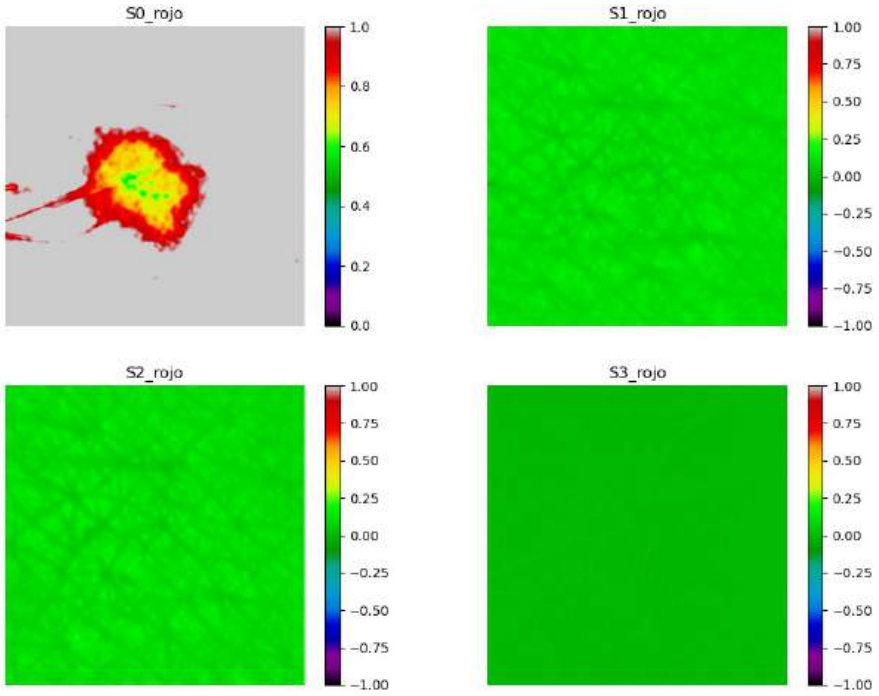

Figure 4.12 – Stokes parameters with linearly polarized red light at 45 degrees.

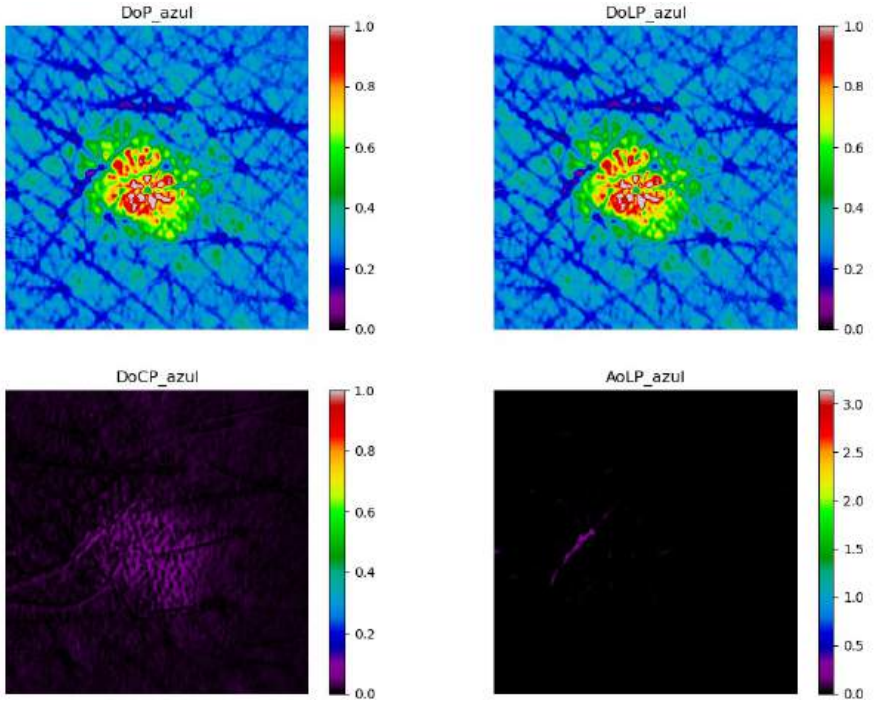

Figure 4.13 – Degree of Polarization (DoP), Degree of Linear Polarization (DoLP), Degree of Circular Polarization (DoCP), and Angle of Linear Polarization (AoLP) with linearly polarized blue light at 45 degrees.

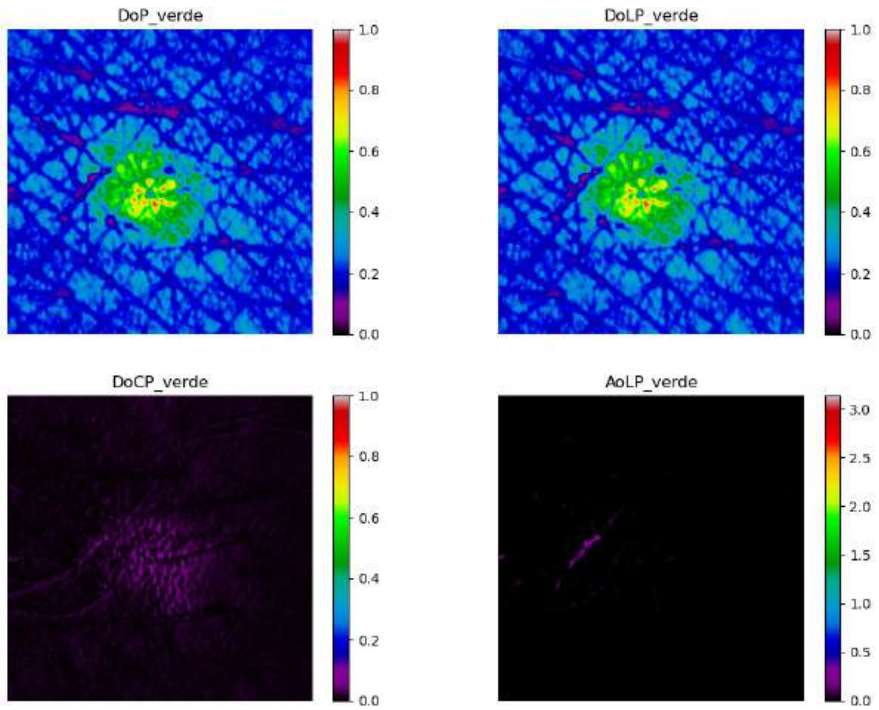

Figure 4.14 – Degree of Polarization (DoP), Degree of Linear Polarization (DoLP), Degree of Circular Polarization (DoCP), and Angle of Linear Polarization (AoLP) with linearly polarized blue light at 45 degrees.

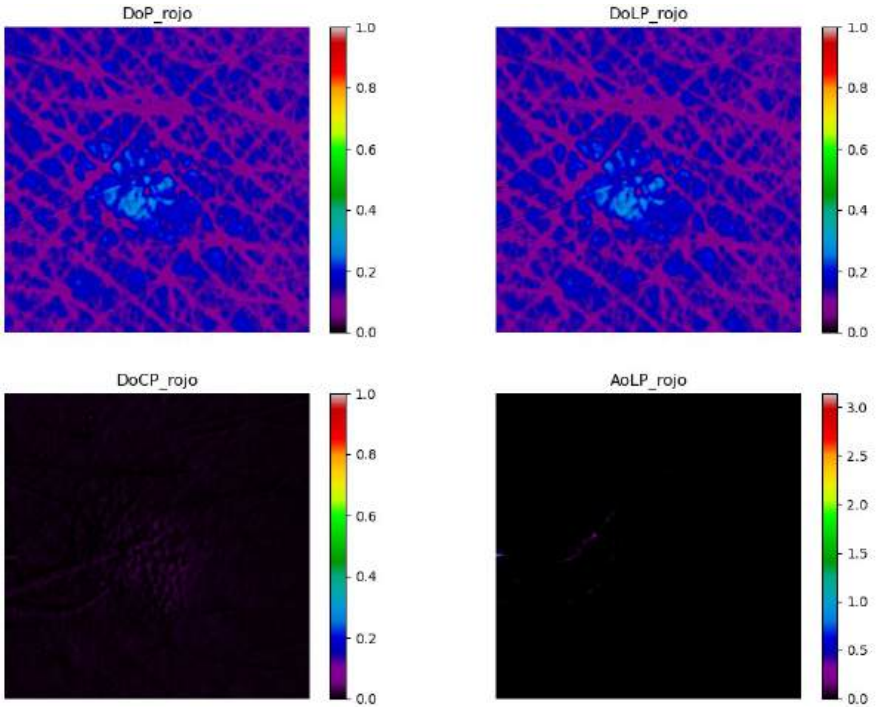

Figure 4.15 – Degree of Polarization (DoP), Degree of Linear Polarization (DoLP), Degree of Circular Polarization (DoCP), and Angle of Linear Polarization (AoLP) with linearly polarized blue light at 45 degrees.

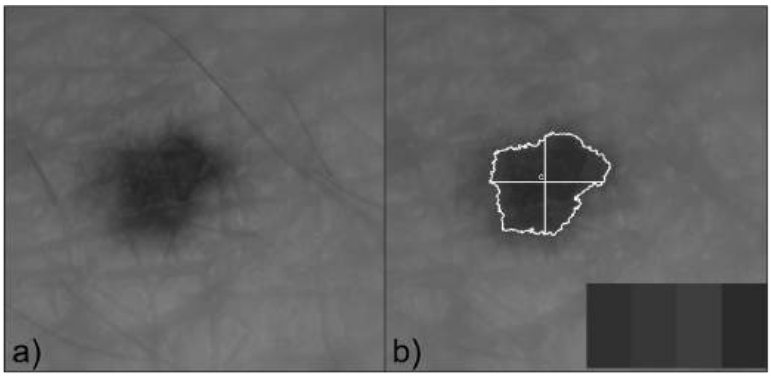

Figure 4.16 – Input and output image for the ABCDE rule.

```
A: Asymmetry Index (max 6%): 17.73% - Dangerous
B: Border Irregularity (max 1.8): 5.38 - Dangerous
C: Color Variation (max 30%): 24.71% - Safe
D: Diameter (max 6mm): 2.02 mm - Safe
```

Figure 4.17 – Obtained ABCDE parameters

4.4 ABCDE parameters aquisition

Another important feature of the project is the automatic extraction and quantification of the ABCDE parameters. The only input needed to obtain all the information for this process is the image taken with white illumination. The program then automatically identifies two axes of symmetry, the border, and the color palette of the mole. With this information, the ABCD parameters can be mathematically calculated, displayed, and saved by the program (for the E parameter). The input and output images are shown in Figure 4.17.

The parameters are then quantified and a preliminary threshold for each one is shown. If the calculated value exceeds the given threshold, then the program will indicate that it is “dangerous”, but if it is below the threshold, then the program will print “safe”. This result is shown in Figure 4.17

Chapter 5

Discussion

5.1 Closing remarks

The device successfully obtained the Stokes parameters and polarization degrees, showing a clear difference in the results based on the color used for sample illumination and also showing differences between the types of polarization used. Through the integration of polarimetric imaging techniques and digital image processing, this handheld device offers a user-friendly and portable tool for physicians to improve the quality of melanoma diagnosis. Additionally, with the inclusion of not only the polarimetric images but also the quantification of the ABCDE rule, it provides the necessary tools to build a database of polarimetric images of the skin, offering new information for the development of machine learning algorithms for the classification of moles and the automatic detection of melanoma.

As with any engineering project, the device can be upgraded incrementally, such as reducing image capture time or making it wireless. However, those upgrades can be implemented in future versions or even as more "premium" features for the final user. Nonetheless, the device is completely finished and ready to use. Combining different aspects and techniques of optical and mechatronic techniques, this is a finished, fully functional optomecathronic project.

This optomechatronic project represents a significant advancement in dermatological imaging, offering an effective tool for both use in uncontrolled environments and research.

With continued development and validation, it will potentially improve skin cancer detection, hopefully reducing the deaths caused by melanoma and maybe inspiring the development of similar devices for other types of cancers.

5.2 Future work: Improvements, additions and discards

As with any engineering work, there are always possible improvements that can be made, which in this case would remain as future work. The most relevant points in this regard are:

- Partner with a dermatologist to conduct clinical trials, and to get validation.
- Build a database of polarimetric images.
- Reduce the image capture time.
- Develop a device that includes infrared illumination.
- Use artificial intelligence algorithms to classify moles as potentially malignant or benign.
- Develop a wireless device.
- Create a more robust user interface with additional functionalities.

List of References

[1] A. Dabrowska, F. Spano, S. Derler, C. Adlhart, N. Spencer, and R. Rossi, "The relationship between skin function, barrier properties, and body-dependent factors," *Skin Research and Technology*, vol. 24, no. 2, pp. 165–174, 2018.

[2] J. Zwirner and N. Hammer, "Anatomy and physiology of the skin," in *Scars*, S. P. Nischwitz, L. Kamolz, and L. K. Branski, Eds. Springer, 2024.

[3] H. Yousef, M. Alhajj, A. O. Fakoya, and S. Sharma, "Anatomy, skin (integument), epidermis." [Online]. Available: https://www.ncbi.nlm.nih.gov/books/NBK470464/

[4] R. Lapides *et al.*, "Possible explanations for rising melanoma rates despite increased sunscreen use over the past several decades," *Cancers*, vol. 15, pp. 495–503, 2023.

[5] W. H. Organization, "Radiation: Ultraviolet (uv) radiation and skin cancer," 2017, accessed 29 April 2024. [Online]. Available: https://www.who.int/news-room/questions-and-answers/item/radiation-ultraviolet-(uv)-radiation-and-skin-cancer

[6] N. Iglesias-Pena, S. Paradela, A. Tejera-Vaquerizo, A. Boada, and E. Fonseca, "Cutaneous melanoma in the elderly: Review of a growing problem," *Actas Dermo-Sifiliográficas (English Edition)*, vol. 110, no. 6, pp. 434–447, 2019.

[7] R. Naheed *et al.*, "Early diagnosis of cutaneous melanoma. revisiting the abcd criteria," *Clinical's Corner*, vol. 292, no. 22, pp. 2771–2776, 2004.

[8] H. Kittler, "Evolution of the clinical, dermoscopic and pathologic diagnosis of melanoma," *DPC Journal Special Issue Melanoma Today*, 2021.

[9] A. F. Duarte, B. Sousa-Pinto, L. F. Azevedo, A. M. Barros, S. Puig, J. Malvehy, E. Haneke, and O. Correia, "Clinical ABCDE rule for early melanoma detection," *European Journal of Dermatology*, vol. 31, pp. 771–778, 2021.

[10] N. M. Congdon and C. M. Davis, "A systematic review of the frequency of features of the seven-point checklist in proven cutaneous melanoma: The importance of change," *Skin Health and Disease*, vol. 3, p. e295, 2023.

[11] E. Z. Keung, C. M. Balch, J. E. Gershenwald, and A. C. Halpern, "Key changes in the AJCC eighth edition melanoma staging system," *The Melanoma Letter*, vol. 36, pp. 1–9, 2018.

[12] A. Waldmann. *et al.*, "Skin cancer screening participation and impact on melanoma incidence in germany–an observational study on incidence trends in regions with and without population-based screening," *Br J Cancer.*, vol. 106, pp. 970–974, 2012.

[13] Kagle. (2023) Skin cancer (PAD-UFES-20). [Online]. Available: https://www.kaggle.com/datasets/mahdavi1202/skin-cancer

[14] The International Skin Imaging Collaboration (ISIC). (2021) The ISIC 2020 challenge dataset: Skin lesion analysis towards melanoma detection. [Online]. Available: https://challenge2020.isic-archive.com/

[15] P. Tschandl, "The HAM10000 dataset, a large collection of multi-source dermatoscopic images of common pigmented skin lesions," 2018. [Online]. Available: https://doi.org/10.7910/DVN/DBW86T

[16] Y. Castillejos, "Dermatoscopio multiespectral basado en luz polarizada," Master thesis, Centro de Investigaciones en Óptica A.C., December 2017.

[17] M. Mata, "Metodología para identificar ventajas competitivas y elementos de diferenciación en un producto: Dermatoscopio multiespectral." Master thesis, Universidad de Guadalajara, 2022.

[18] L. Jütte *et al.*, "Registration of polarimetric images for in vivo skin diagnostics," *Journal of Biomedical Optics*, vol. 27, pp. 096 001–1–096 001–16, 2022.

[19] A.-R. H. Ali *et al.*, "Automating the ABCD rule for melanoma detection: A survey," *IEEE Acces*, vol. 8, pp. 83 333–83 346, 2020.

[20] S. Gupta *et al.*, "Cognitive-inspired and computationally intelligent early melanoma detection using feature analysis techniques," *Journal of Artificial Intelligence and Technology*, vol. 3, no. 4, pp. 215–223, 2023.

[21] Y. Liuqing, "Multi-spectrum portable dermatoscope system," China Application Number 102016000564379, Jul. 2016.

[22] R. Uthoff and R. Liang, "Smartphone-based multispectral dermascope," International Patent Application Number PCT/US2021/054129, Oct. 2021.

[23] Y. Zhen and C. Xuelian, "Dermatoscope image recognition method and device," China Patent Application Number 202010455685.4, May. 2023.

[24] Y. Liuqing, "Medical multispectral dermatoscope system," China Patent Application Number 201610565047.1, May. 2020.

[25] M. Weimin and C. Deyang, "Multispectral local microscopic amplification 3d dermatoscope device," China Patent Application Number 202221982592.8, July 2023.

[26] D. H. Goldstein, *Polarized Light*, 3rd ed. CRC Press, Jan. 2017.

[27] V. Barun. *et al.*, "Absorption spectra and light penetration depth of normal and pathologically altered human skin. revisiting the ABCD criteria," *Journal of Applied Spectroscopy*, vol. 74, no. 3, pp. 430–439, 2004.

[28] A. Caerwyn *et al.*, "Effect of wavelength and beam width on penetration in light-tissue interaction using computational methods," *Lasers in Medical Science*, vol. 32, no. 4, pp. 1909–1918, 2017.

[29] J. Koehoorn, A. C. Sobiecki, D. Boda, A. Diaconeasa, S. Doshi, S. Paisey, A. Jalba, and A. Telea, "Automated digital hair removal by threshold decomposition and morphological analysis," in *Mathematical Morphology and Its Applications to Signal and Image Processing*, J. A. Benediktsson, J. Chanussot, L. Najman, and H. Talbot, Eds. Cham: Springer International Publishing, 2015, pp. 15–26.

[30] K. Delibasis, K. Moutselos, E. Vorgiazidou, and I. Maglogiannis, "Automated hair removal in dermoscopy images using shallow and deep learning neural architectures," *Computer Methods and Programs in Biomedicine Update*, vol. 4, p. 100109, 2023.

[31] D. Hernández-López, "Módulo de iluminación LED con estándar de reflexión difusa para la caracterización espectroscópica de materiales automotrices," Master thesis, Centro de Investigaciones en Óptica, A. C., 2019.

Appendix A

Prototype components: Spectral features

A.1 Linear polarizing filters

High Contrast Linear Polarizing Film (XP42) and Ultra High Contrast Visible Dichroic Polarizer were purchased from Edmund Optics and Bolder Vision Optik, respectively. Transmittance spectra show that optical component placed at the imaging Stokes polarimeter absorbs less light over the visible range.

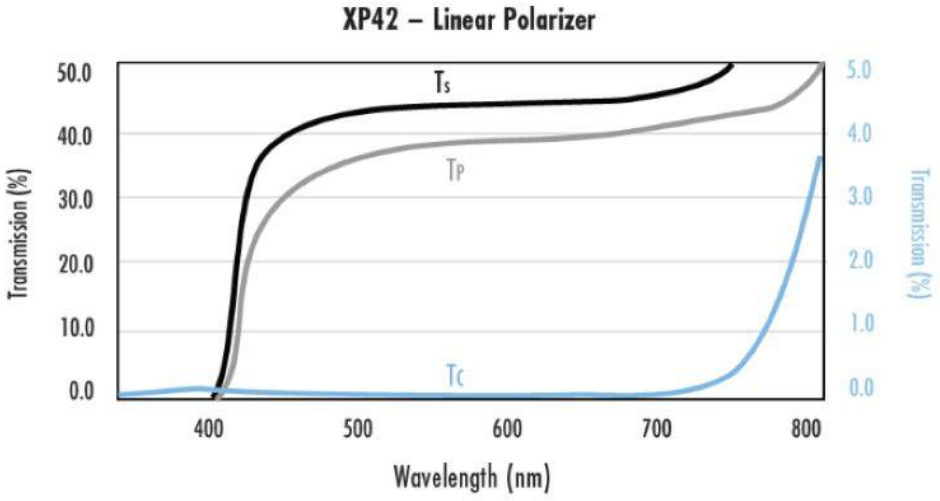

Figure A.1 – Transmittance of the linear polarizing film used in the RGB illumination source. Adapted from https://www.edmundoptics.com/f/high-contrast-linear-polarizing-film/14385/

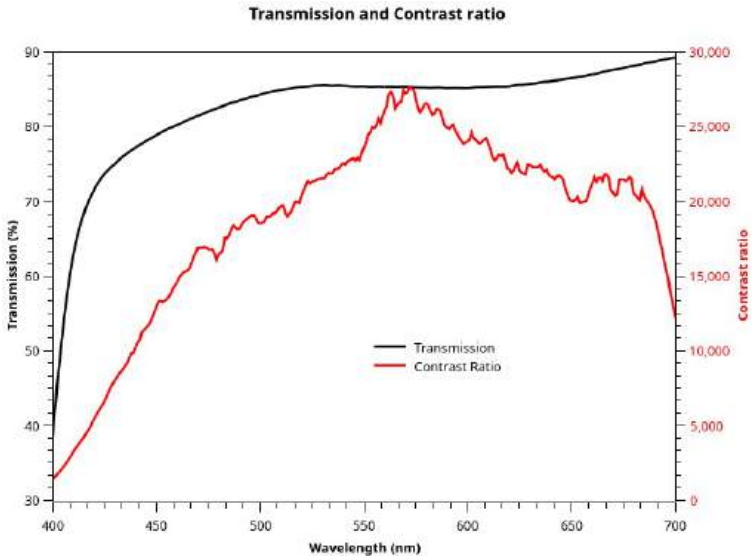

Figure A.2 – Transmittance and constrast ratio of the linear polarizing plate used in the imaging Stokes polarimer. Adapted from https://boldervision.com/linear-polarizers/bvo-uhc-polarizer/

A.2 Quarter-wave retarders

Birefringent Polymer $\lambda/4$ Retarder Film (WP140HE) and Visible Achromatic Quarterwave Retarder (AQWP3) were purchased from Edmund Optics and Bolder Vision Optik, respectively. Retardance spectra show a better performance of the birefringent component used in the imaging Stokes polarimeter all over the visible range.

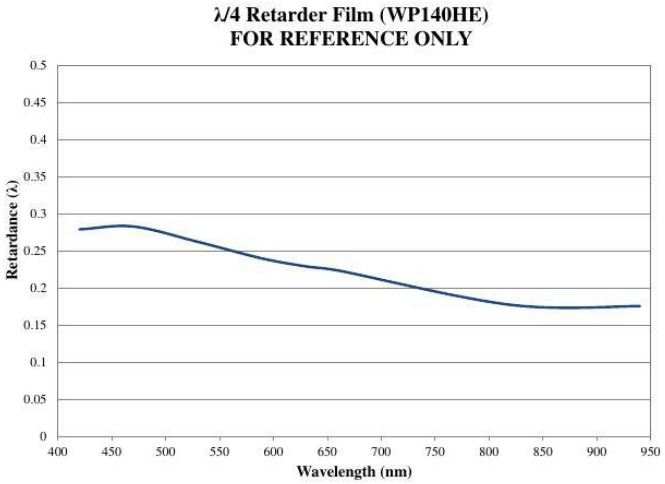

Figure A.3 – Retardation of the birefringent film used in the illumination source. Adapted from https://www.edmundoptics.com/f/polymer-retarder-film/14827/

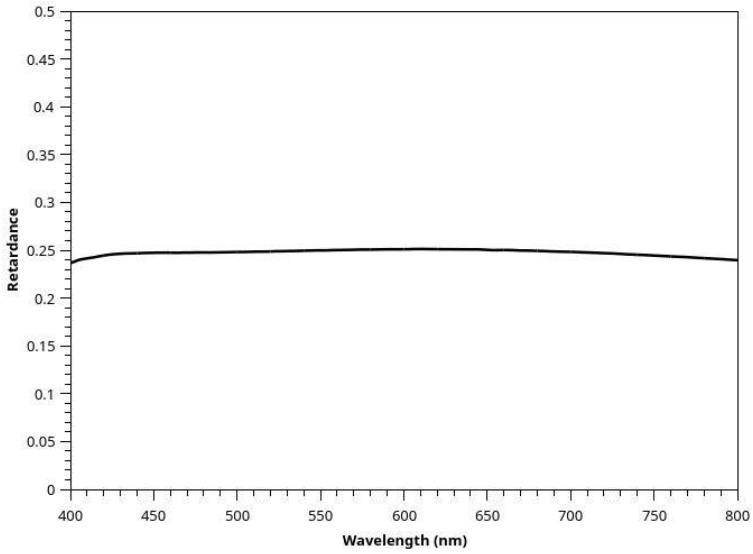

Figure A.4 – Retardation of the birefringent plate used in the imaging Stokes polarimeter. Adapted from https://boldervision.com/waveplates/aqwp3/

A.3 CMOS array monochromatic sensor

The imaging acquisition device used in the prototype was a Basler daA1920-160um (No-Mount) USB 3.0 camera with the Sony IMX392 CMOS sensor, which delivers 160 frames per second at 2.3 MP resolution. It is noted that relative spectral sensitivity is above 0.3 in the visible range with a maximum around 600 nm.

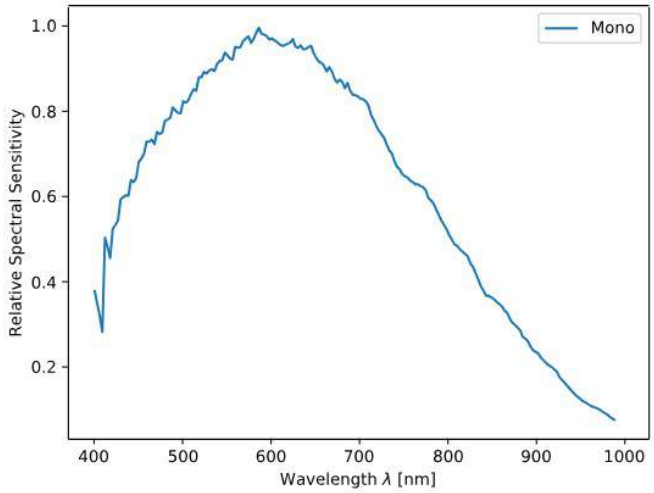

Figure A.5 – Spectral response curve of the monochromatic CMOS array sensor. Adapted from https://docs.baslerweb.com/daa1920-160um

A.4 Imaging lenses

Focal length shift and wavefront error as a function of wavelength are parameter related to imaging lens performance. It can be observed that, as demonstrated in the ray tracing analysis, distortions are compensated by combining these achromatic doublets (cemented and air spaced).

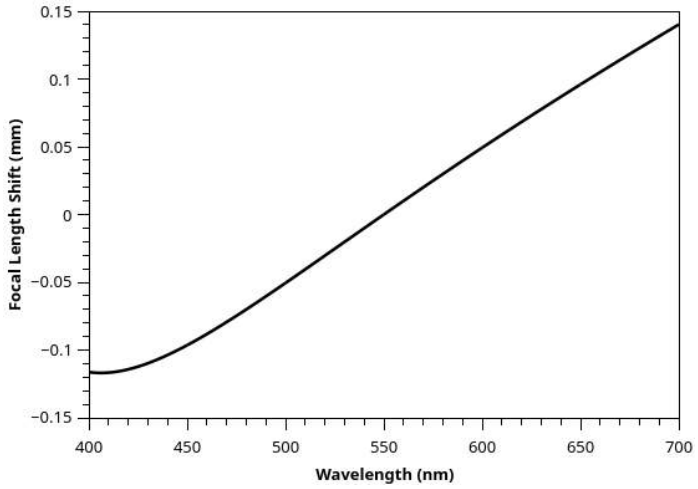

Figure A.6 – Focal length shift as a function of wavelength for the cemented achromatic doublet lens. Adapted from https://www.thorlabs.com/newgrouppage9.cfm?objectgroup_id=2696&pn=AC254-040-A-ML#3441

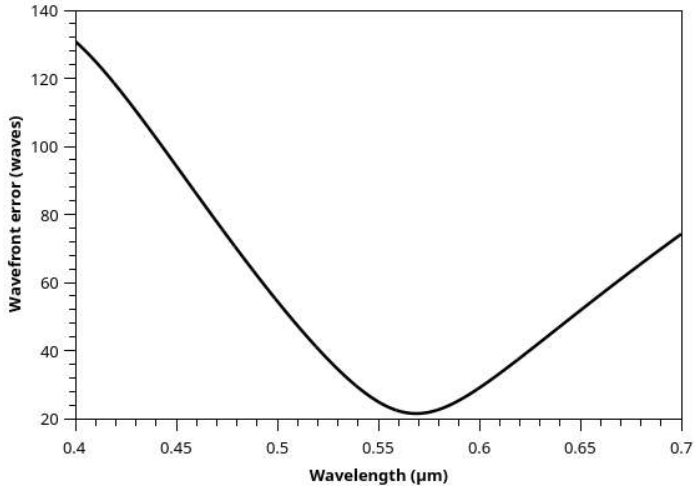

Figure A.7 – Wavefront error as a function of wavelength for the air-spaced achromatic doublet lens. Adapted from https://www.thorlabs.com/newgrouppage9.cfm?objectgroup_id=6083&pn=ACA254-030-A#6784

A.5 RGB ring lamp

An addressable ring lamp comprising 16 RGB-LED elements arrange in a circle produce the different illumination settings. Spectra for white, red, green and blue illumination ranges are shown below, which were measured with a USB4000 Fiber Optic Spectrometer.

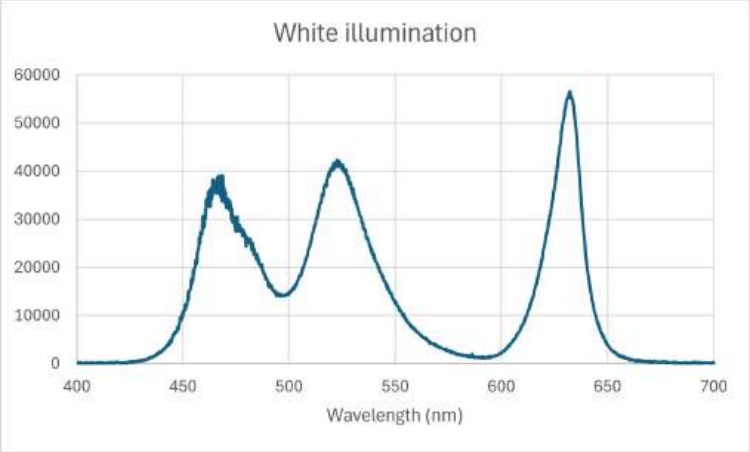

Figure A.8 – White light spectrum emitted by the illumination source. Three emitters in each RGB-LED are excited simultaneously.

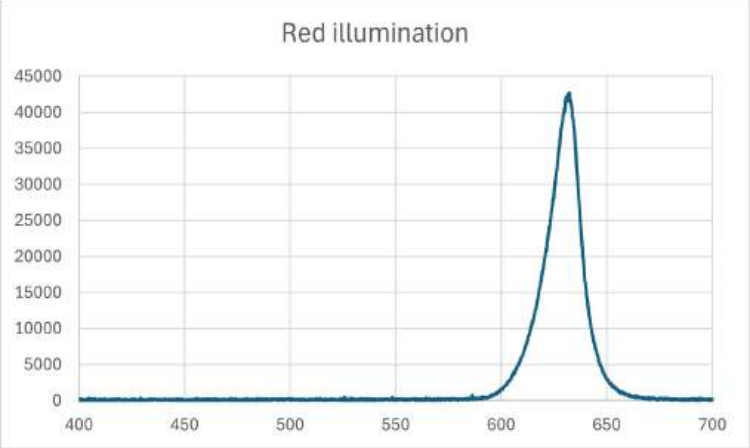

Figure A.9 – Spectrum of red emission centered at 625 nm with a bandwidth of approximately 15 nm.

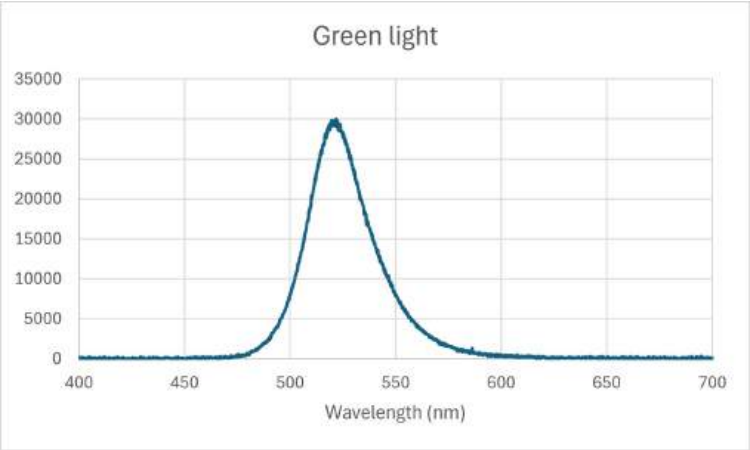

Figure A.10 – Spectrum of green emission centered at 520 nm with a bandwidth of approximately 35 nm.

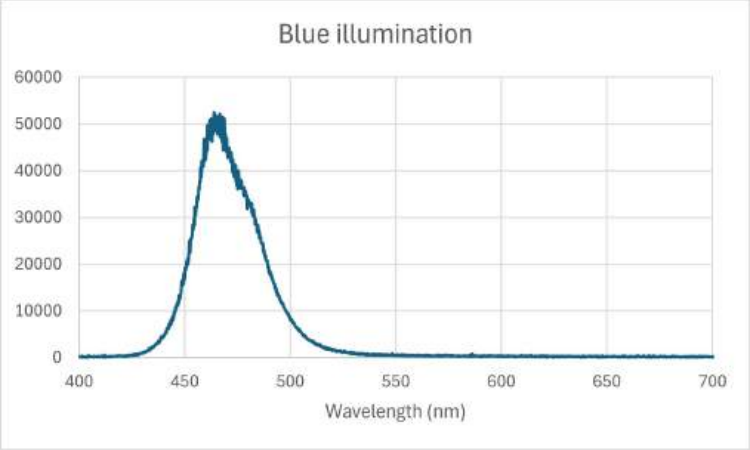

Figure A.11 – Spectrum of blue emission centered at 465 nm with a bandwidth of approximately 30 nm.